Europe PMC Funders Group
Author Manuscript
Adv Drug Deliv Rev. Author manuscript; available in PMC 2018 September 10.

Published in final edited form as:
Adv Drug Deliv Rev. 2017 November 01; 121: 9–26. doi:10.1016/j.addr.2017.10.013.

Fibrosis imaging: Current concepts and future directions

Maike Baues[a], **Anshuman Dasgupta**[a], **Josef Ehling**[a], **Jai Prakash**[b], **Peter Boor**[c], **Frank Tacke**[d], **Fabian Kiessling**[a], and **Twan Lammers**[a,b,e,#]

[a]Department of Nanomedicines and Theranostics, Institute for Experimental Molecular Imaging, Uniklinik RWTH Aachen and Helmholtz Institute for Biomedical Engineering, RWTH Aachen University, 52074 Aachen, Germany [b]Department of Targeted Therapeutics, MIRA Institute for Biomedical Technology and Technical Medicine, University of Twente, 7500 AE Enschede, The Netherlands [c]Department of Nephrology and Institute of Pathology, Uniklinik RWTH Aachen, RWTH Aachen University, 52074 Aachen, Germany [d]Department of Medicine III, Uniklinik RWTH Aachen, RWTH Aachen University, 52074 Aachen, Germany [e]Department of Pharmaceutics, Utrecht Institute for Pharmaceutical Sciences, Utrecht University, 3584 CG Utrecht, The Netherlands

Abstract

Fibrosis plays a role in many different pathologies. It results from tissue injury, chronic inflammation, autoimmune reactions and genetic alterations, and it is characterized by the excessive deposition of extracellular matrix components. Biopsies are routinely employed for fibrosis diagnosis, but they suffer from several drawbacks, including their invasive nature, sampling variability and limited spatial information. To overcome these limitations, multiple different imaging tools and technologies have been evaluated over the years, including x-ray imaging, computed tomography (CT), ultrasound (US), magnetic resonance imaging (MRI), positron emission tomography (PET) and single-photon emission computed tomography (SPECT). These modalities can provide anatomical, functional and molecular imaging information which is useful for fibrosis diagnosis and staging, and they may also hold potential for the longitudinal assessment of therapy responses. Here, we summarize the use of non-invasive imaging techniques for monitoring fibrosis in parenchymal organs such as liver, kidney, lung and heart, in systemic autoimmune diseases and in desmoplastic cancers, and we discuss how imaging biomarkers can be integrated in (pre-) clinical research to individualize and improve anti-fibrotic therapies.

1 Introduction

Fibrosis is a common feature in many different pathologies. It is characterized by the accumulation of extracellular matrix (ECM) components and is associated with up to 45% of deaths in industrialized countries [1]. In general, fibrosis mechanisms include exacerbated injury-related responses that are dysregulated versions of conventional tissue repair processes [2]. Core elements in disease progression can be acute, recurrent or persistent epithelial and endothelial injuries that can both initiate and sustain fibrosis [3]. These

[#]Corresponding author: tlammers@ukaachen.de.

Europe PMC Funders Author Manuscripts
Europe PMC Funders Author Manuscripts

Europe PMC Funders Author Manuscripts

Europe PMC Funders Author Manuscripts

pathogenic pathways furthermore involve changes in numerous inflammatory, endothelial and mesenchymal cells, resulting in increased production of fibronectin, osteopontin, hyaluronan, proteoglycans, laminins and a variety of collagen subtypes [4]. The abnormal ECM deposition which is typical of fibrosis leads to a disruption and distortion of the tissue architecture and function [5]. These fundamental fibrotic processes are shared across a variety of tissues and organs, including connective tissue, gastrointestinal tract, liver, kidney, lung and heart (Fig. 1). While the mechanisms of fibrogenesis are similar, the regenerative capacity and the ability to reverse advanced fibrosis vary tremendously [6]. Resolution of fibrosis is for example possible in the liver when the underlying cause is removed; this is for instance the case in complete suppression of hepatitis B virus replication and curative treatment of hepatitis C [7, 8].

The desmoplastic reaction and increased ECM production in tumors is remarkably similar to organ fibrosis [9]. Cancer-associated fibroblasts (CAF) are one of the most crucial components of the tumor microenvironment and have been implicated in angiogenesis, immunosuppression and metastasis [10, 11]. Fibrotic stroma affects disease progression in various tumors, e.g. breast cancer, in colon/colorectal cancer and in pancreatic tumors, as well as in head and neck cancer [12, 13].

In contrast to fibrosis as a common endpoint for all of the above organs and tissues, the etiologies causing fibrosis are highly diverse, encompassing an array of different triggers such as acute injury, chronic inflammation, autoimmune reactions and genetic alterations. In some cases, the exact etiology may even remain unknown. While a detailed description of these triggers and their disease-initiating mechanisms is beyond the scope of this review, several prototypic examples can be provided, to exemplify the high prevalence and far-reaching consequences of fibrotic processes in human diseases. Among the most obvious etiologies for induction of fibrosis are exposure to ionizing irradiation and mechanical obstruction, resulting from e.g. myocardial infarction, surgical intervention, gall- and kidney-stones. Frequently accountable chronic illnesses with fibrotic elements include psoriasis, Crohn’s disease, pneumoconiosis subtypes, steatohepatitis, viral hepatitis and glomerulosclerosis. Also many autoimmune disorders, such as rheumatoid arthritis, systemic lupus erythematosus, Sjörgen’s syndrome, progressive systemic sclerosis, Hashimoto’s thyroiditis and ankylosing spondylitis are associated with fibrosis. Underlying genetic predispositions that make individuals susceptible to fibrosis are neurofibromatosis, cystic fibrosis, alpha 1-antitrypsin deficiency, tyrosinosis, Wilson’s disease and hemochromatosis, as well as hypertrophic and restrictive cardiomyopathy. There are multiple fibrosis-related diseases, in which the exact triggers are unknown, such as sarcoidosis, idiopathic pulmonary fibrosis, retroperitoneal fibrosis, acute interstitial pneumonitis and dilated cardiomyopathy. A summary of triggers and of the resulting pathophysiological changes for the most commonly affected tissues and organs is provided in Fig. 2.

Accurate diagnosis and staging of fibrosis is essential for proper prognosis and progression monitoring. The presence and severity of fibrosis actually are the best predictor for disease progression in chronic kidney disorders [14] as well as in fatty liver disease [15]. Traditionally, needle-based biopsies have been the gold standard for fibrosis diagnosis and staging. Biopsies, however, are faced with multiple limitations including their invasive

Europe PMC Funders Author Manuscripts

Europe PMC Funders Author Manuscripts

nature, procedure-associated risks, limited representativeness for the entire organ, and inter- and intra-observer sampling variability [16].

In the recent years, increasing numbers of studies have focused on the development of non-invasive imaging techniques for fibrosis diagnosis, staging and treatment monitoring. Non-invasive imaging techniques such as ultrasound (US), magnetic resonance imaging (MRI), x-ray imaging, computed tomography (CT), optical imaging (OI), positron emission tomography (PET) and single-photon emission computed tomography (SPECT) have all been employed for this purpose [17–21].

In the present review, we summarize exemplary studies illustrating the use of anatomical, functional and molecular imaging techniques for fibrosis diagnosis and staging. We also discuss the potential of using imaging biomarkers to facilitate translational research, and to individualize and improve anti-fibrotic therapies.

2 Biopsies and liquid biomarkers to assess fibrosis

An accurate determination of fibrosis stage is crucial for the prediction of prognosis, for determining surveillance strategies and for selecting a suitable therapeutic approach. Traditionally, needle-based biopsies are considered the gold standard and they often are the only available means for specific fibrosis assessment and exact disease differentiation.

In the case of systemic lupus erythematosus (SLE), for instance, a renal biopsy is crucial to diagnose the specific form of lupus [22]. In general, multiple stainings can be employed for visual inspection, such as hematoxylin and eosin staining or more specifically trichrome or Sirius Red stainings (marking collageneous fibers) or immunohistochemistry specific for certain types of collagens or other ECM components [23].

To achieve optimal accuracy in the diagnosis of fibrosis, the biopsy bias has to be minimized, starting with the excised sample, which should have specific properties. An adequate kidney biopsy is 10 mm in length and at least 1.2 mm in width, and it should contain 10-15 glomeruli [24]. A liver biopsy is considered adequate if it has a length of at least 20 mm and contains at least 11 portal tracts (some experts even prefer 16 portal tracts) [25]. However, such “optimal” liver biopsies only represent 1/50,000 of the total liver volume [26]. For the diagnosis of arthritic diseases, a biopsy sample of the synovial fluid is considered as equivalently informative as a sample of the synovial tissue [27]. The diagnosis of connective tissue disease is commonly performed on the basis hematological tests (complete blood count, erythrocyte sedimentation rate), biochemical analysis (C-reactive protein, hepatic function, renal function) and immunologic investigations (autoantibodies, rheumatoid factors, antinuclear antibodies, antibodies to DNA, antiphospholipid antibodies) [27, 28].

In case of tumors, a biopsy is the standard diagnostic procedure to determine the nature and stage of the tumor, as well as its malignant potential. Although the essential role of desmoplastic processes for tumor growth and metastasis has been recognized [29], they are not considered in routine pathological assessments. Many studies have suggested that especially in invasive colorectal cancer [30–32] and in pancreatic ductal adenocarcinoma

Europe PMC Funders Author Manuscripts

Europe PMC Funders Author Manuscripts

[33–35], the desmoplastic reaction is a key hallmark determining therapeutic outcome. Thus far, however, histopathological information on e.g. myxoid stroma as an indicator for epithelial-to-mesenchymal transition [30], has not yet managed to become broadly accepted and implemented for disease differentiation, prognosis assessment and treatment selection [36].

While needle-based biopsies inevitably play an important role in the diagnosis and staging of fibrotic diseases, they suffer from several drawbacks, including invasiveness with the risk of life-threatening complications, sampling errors, and intra- and inter-observer variability [37, 38]. Moreover, repeated biopsy procedures are difficult and impractical, due to the increased risk of complications [39]. Nevertheless, because of the lack of reliable tools and technologies to obtain information non-invasively, up to 4 biopsies are still routinely taken in large phase III trials, e.g. in patients suffering from non-alcoholic steatohepatitis (NASH) [40].

In tumors, biopsy-based diagnosis is particularly complicated, because of intrinsic heterogeneity in the primary tumor, as well as heterogeneity between the primary tumor and metastases [41]. In such situations, also the accessibility of the pathological site(s) and the risk of spreading/seeding cancer cells play an important role [42]. In light of these limitations, liquid biopsies are increasingly emerging in the field of cancer diagnosis as a refined and non-invasive alternative (and/or as an add-on) to needle-based biopsies [43]. A liquid biopsy, in the form of a blood sample, can provide information on the genetic profile of cancerous lesions (and the heterogeneity therein) by means of analyzing circulating tumor cells or circulating cell-free tumor DNA [44, 45].

Because of their high applicability, reproducibility and widespread availability, liquid-based biopsies not only hold great promise for cancer diagnosis, but also for the assessment of classical fibrotic diseases. For the assessment of liver fibrosis, for instance, several serum biomarkers are available that are composite scores of not strictly liver-specific parameters as well as some that have been associated with fibrosis stage, but both types have been mainly proposed for patients with chronic hepatitis C [46]. The most commonly used tests include the FibroTest® (which combines alpha-2 macrolobulin, haptoglobin, apolipoprotein, bilirubin, gamma glutamyle transferase, age and gender into an algorithm), the aspartate-to-platelet ratio index (APRI) and the Enhanced Liver Fibrosis score (ELF; which includes amino-terminal propeptide of procollagen type III (PIIINP), TIMP metallopeptidase inhibitor 1 and hyaluronic acid) [46–48].

In kidney fibrosis, liquid biopsy-based biomarkers can be measured in blood as well as in urine. In this regard, the correlation of transforming-growth factor-β (TGF-β) and bone morphogenetic protein-7 (BMP-7) levels in both blood and urine has been to correlate well with the degree of fibrosis [49]. Additionally, the urinary ratio of the N-terminal propeptide of collagen III (Pro-C3) to the the MMP-generated collagen III degradation fragment (C3M) has been identified to reflect ECM turnover in multiple rat models as well as in patients suffering from IgA nephropathy [50, 51]

Europe PMC Funders Author Manuscripts

Europe PMC Funders Author Manuscripts

For staging and prognosis assessment in lung fibrosis, serum levels of the glycoprotein Krebs von Lungen-6 (KL-6) [52] and of the surfactant proteins A and D have been shown to be useful, as they are clearly elevated during disease progression [53]. In addition to blood, also bronchoalveolar lavage samples can be used as liquid biomarkers, correlating MMP1 and MMP7 to disease severity [54].

In cardiac fibrosis many circulating molecules have been proposed and validated as serum biomarkers [55, 56]. However, only two circulating collagen-derived peptides, i.e. the carboxy-terminal propeptide of procollagen type I (PIP) [57] and the amino-terminal propeptide of procollagen type III (PIIINP) [58], are proven to be associated with fibrotic processes in the heart [56]. Recently, the potential of circulating microRNAs (miRNAs; i.e short, noncoding RNAs which post-transcriptionally control gene expression), has been evaluated, and miR-29, miR-30 and miR-21 have been identified as promising new liquid biomarkers for cardiac fibrosis [59, 60].

Shortcomings of liquid-based biomarkers are that they may not be organ-specific (enough), that they may be limited to the indication of impaired organ function or inflammatory state, and in particular that they may not specifically reflect fibrosis or discriminate between different stages of fibrosis [61, 62]. The abovementioned new biomarkers may help to provide more fibrosis-specific information, since they mostly assess molecules of the ECM. These novel markers now require validation in large cohorts of patients and in long-term studies [62]. In the future, such liquid biopsy techniques may be used in combination with other modalities, such as imaging, to improve the accuracy of fibrosis diagnosis and staging.

Another appealing approach for the assessment of fibrosis is via noninvasive imaging. Anatomical, functional and molecular imaging techniques allow for the examination of the entire affected organ (or even the whole body), in a readily repeatable manner. In the case of fibrosis, this makes them attractive for staging and progression monitoring. In addition, these techniques can also be readily employed for repetitive treatment monitoring, thereby potentially facilitating the clinical translation of novel anti-fibrotic therapies.

3 Non-invasive imaging of fibrosis

3.1 Autoimmune-related fibrosis

Accurate diagnosis is challenging in the early course of autoimmune- and connective tissue-related fibrosis because of their very versatile clinical presentation. This is further complicated by the fact that symptoms are never really specific for one of the many possible autoimmune connective tissue diseases [63]. This exemplifies the need for imaging technologies able to differentiate between different autoimmune disease and disease stages.

The plain acquisition of typical structural changes in connective tissues via clinically established imaging modalities may already be very helpful to support a certain diagnosis. For instance, in the diagnosis of ankylosing spondylitis, an inflammatory condition of the joints and the enthuses of the spine, accompanied by paraspinal muscle fibrosis [64], the role of anatomical MRI is very prominent, because in common radiography as well as in CT images, structural changes may only become visible at later stages, when the lesions are

Europe PMC Funders Author Manuscripts

Europe PMC Funders Author Manuscripts

already chronic [65]. The early recognition of inflammation with MRI and the possibility of whole spine imaging (enabling sagittal and coronal assessment within max. 30 min) [66], has led to the inclusion of MRI in the new classification criteria by the Assessment of Spondylarthritis International Society [67]. The inflammatory reaction of the spine appears in MRI with high signal intensity on short tau inversion recovery (STIR) and T2 fat saturated sequences (Fig. 3A-B) as well as T1 fat saturated sequences after administration of gadolinium-based contrast agents [68]. Typically inflammatory lesions are visible at the corners of the vertebral bodies or edema can also be detected throughout or central of the intervertebral space [69]. However, these MRI pattern also present in degenerative diseases and spinal metastases, therefore such findings need to be examined in closer detail and should be confirmed with another noninvasive imaging modality [70]. Ultrasonography could be such a tool for the diagnosis of ankylosing spondylitis, as it can provide more fibrosis-related information on peripheral joints and entheses [68]. For example, on B-mode US images, tendon thickening is detected as decreased echogenic areas as well as enthesophytic structures [71]. The assessment of fibrosis can be improved in case of functional imaging by applying power Doppler US.

Recent advances in functional sonography have made it the most widely applied imaging modality for the diagnosis of inflammatory joint disease, and they have had major impact on the evaluation of patients with early rheumatoid arthritis, enabling the detection of pre-erosive synovitis [72]. Abnormal hypoechoic and uncompressible tissue can be seen in grey-scale/B-mode US images [73]. Besides providing anatomical information on soft tissue changes and on the thickening of the synovial membrane, power Doppler US can also assess functional features such as synovial blood flow [74] and it can distinguish between disease activity levels [75] as well as differentiate low arthritis activity from clinical remission [76]. High signal intensities in Doppler US imaging are characteristic of a hypervascularized pannus tissue in fibrosis [77]. Over the past years, different scoring systems have been developed to standardize clinical findings [78]. Based on the four-step semiquantitative US grading system, developed by Szkudlarek et al., [79] the color Doppler US image in Fig. 3C exemplifies a wrist joint of a healthy patient, and the counter piece in Fig. 3D a joint of a patient suffering from severe rheumatoid arthritis [80]. The latter is identified as grade 3 arthritis, the severest category, because more than half of the area is vascularized and highly perfused, which is indicated by the light blue color coding. The results are comparable with MRI findings and the development of an internationally accepted scoring system would make musculoskeletal US an even more reliable, bedside method for day-to-day clinical practice [81, 82]. The addition of microbubbles as US contrast agents may further improve the detection of neoangiogenesis in fibrotic tissues [83]. Issues regarding the number of joints to be examined and the resulting time constraints were resolved with the establishment of a 7-joint US score (German US7 score). By focusing on a small but conclusive number of active joint regions, the repeatability of the procedure and integration in daily rheumatologic practice can be ensured [84].

Fluorescent optical imaging (OI) in combination with the administration of the clinically used optical contrast agent indocyanine-green (ICG) is a novel spatiotemporal imaging alternative for the visualization of vasodilation, hypervascularity and capillary permeability in rheumatoid arthritis [85]. The commercial Xiralite® system was the first OI hardware tool

Europe PMC Funders Author Manuscripts

Europe PMC Funders Author Manuscripts

that allowed for the dynamic and simultaneous analysis of ICG accumulation in both hands of arthritis patients, and findings were comparable to those obtained in MRI measurements [86]. Recently, the applicability of OI has also been tested for the visualization of fibrotic alterations in systemic sclerosis (SSc) with Raynaud's phenomenon (Fig. 3E-F) [87]. Pfeil and colleagues divided each hand into 19 segments and visualized and quantified changes in ICG levels. A healthy hand shows no ICG enhancement (Fig. 3E), whereas sensitive and specific detection of ICG enhancement, resulting from fibrosis-related microvascular damage, was observed in patients with SSc (Fig. 3F) [87]. ICG-enhanced OI was also shown to be useful for monitoring the therapeutic response to the vasodilative and anti-inflammatory agent iloprost in 21 patients with SSc-associated Raynaud's phenomenon [88]. Upon further validation, measuring ICG enhancement may turn out to be a fast, sensitive and easy diagnosis and treatment monitoring approach for wide-scale use in SSc and rheumatoid arthritis patients.

The differentiation between systemic lupus erythematosus (SLE) and other autoimmune connective tissue diseases is challenging, because of the mixture of symptoms that may present [89]. The diagnosis of SLE relies mostly on clinical and laboratory features, although imaging would provide insights on organ manifestation especially when the central nervous system is involved [90]. Up to 75% of SLE patients have neuropsychiatric involvement, which is associated with significantly increased morbidity and mortality [91]. Neuropsychiatric lupus erythematosus (NPSLE) is known to be associated with white mater alterations that are often not detectable on routine MRI [92]. Diffusion tensor imaging (DTI) is an advanced functional MRI technique that is sensitive to the microscopic directional diffusion of water molecules through cellular components and thus allows for the analysis of highly cellularly dense tissue such as the brain with its different compartments [93]. In the grey matter water moves isotropically, whereas in the white matter, water molecules diffuse along the length of the axons [94]. DTI enables the characterization of white matter tracts which relate to axon orientation and integrity [95, 96]. In NPSLE patients, this technique can be utilized to detect subtle changes of diffusion anisotropy [97]. DTI indices as well as the number of fiber tracts can assist in finding early signs of pathological involvement and it also holds promise for monitoring disease progression [98]. The color-coded top-view tractograms of a NPSLE patient, who suffered from severe neurological symptoms but had no detectable abnormalities at conventional MRI T1, T2, FLAIR or DWI sequences, before and after steroid pulse therapy (Fig. 3G-H) reveal changes in the white matter integrity [99]. The number of fiber tracts in the frontal lobe significantly increased upon treatment, and this improvement was comparable to the reported clinical signs in this particular patient. Therefore DTI might not only be useful for detecting initial brain involvement in SLE, but also for monitoring early disease progression and treatment effects [98].

Overall, the abovementioned systemic autoimmune disorders have a wide range of presentations, with various overlapping organ manifestations, demanding differential disease diagnosis. Most of the existing imaging techniques focus on inflammatory alterations. If the newly emerging applications would also start to cover fibrosis-related changes, they would have the potential to tremendously improve the diagnosis of rheumatoid and connective tissue diseases. In the near future, these emerging tools may make the diagnosis and management of patients more comprehensive, and they may open up new paths for the

Europe PMC Funders Author Manuscripts

Europe PMC Funders Author Manuscripts

investigation of underlying pathological mechanisms as well as for the evaluation of new treatment possibilities.

3.2 Liver fibrosis

The degree of liver fibrosis is of great importance for proper diagnosis, prognosis assessment and therapeutic intervention in chronic liver disease. Up to now, the histologically determined stage of fibrosis is the strongest independent risk factor for predicting liver-associated complications and the need for liver transplantation, as well as for liver-related and overall mortality [101]. Non-invasive assessment of liver fibrosis has thus far only been established for chronic hepatitis B and C virus infections, via the combination of two concordant tests, i.e. serum biomarkers plus transient elastography [46]. To distinguish between benign fatty liver disease and progressive non-alcoholic steatohepatitis, invasive biopsies are still required [102]. This biopsy procedure comes with multiple drawbacks, including the associated risks, sampling errors and intra- and inter-observer variability. The latter is especially obvious, when semi-quantitative scoring systems are applied, which include grading (steatosis, ballooning, portal inflammation) and staging (fibrosis) [48, 102].

In terms of anatomical imaging, standard gray-scale US is routinely used in the clinic for the assessment of liver disease. It provides baseline information on liver morphology and texture [48]. As an example, Choong and colleagues used gray-scale US to show that the liver surface progressed from being smooth to severely nodularly as the severity of the disease increased (Fig. 4A-B). The authors also reported coarsened echotexture and blunting of liver edges in patients with liver fibrosis. However, this type of anatomical US imaging is limited to the detection of advanced stage fibrosis and does not provide sufficient accuracy for ruling out early-stage liver fibrosis [103]. Besides US, non-contrast-enhanced CT has also been shown to be able to depict liver surface nodularity, and it does so with high accuracy and high intra- and inter-observer independency (upon assistance of an automated computer algorithm). So far, this technique has only been tested retrospectively for the differentiation of cirrhotic from non-cirrhotic livers, and further evaluations are needed to assess its reproducibility, as well as its (prospective) performance in intermediate-stage liver fibrosis [104].

Functional imaging of liver fibrosis has encompassed a variety of elastography modalities, which assess liver stiffness and which have had a massive impact on the non-invasive diagnosis of liver fibrosis. These elastography methods include transient elastography (TE), acoustic radiation force impulse imaging (ARFI), shear wave elastography (SWE) and MR elastography (MRE) [105]. FibroScan® was the first TE device which was approved for the rapid and user-friendly quantification of fibrosis at the bedside [106]. The FibroScan® system consists of an US transducer combined with a vibrator that enables the direct relation of shear wave propagation to tissue stiffness [107, 108]. Initial inaccuracies and even application failures of TE devices in obese patients were partially overcome with an adapted XL probe that allows for deeper tissue penetration [109]. As opposed to TE, both ARFI and SWE use focused US pulses to estimate shear wave velocities in the liver which are related to tissue stiffness. ARFI is based on the elasticity information from the axis of the pushing beam that creates a 2D stiffness map, whereas SWE depends on the shear waves propagating

Europe PMC Funders Author Manuscripts

Europe PMC Funders Author Manuscripts

sideways from the axis of the US beam [110, 111]. Examples for liver SWE scans are depicted in Fig. 4C-D, in which fibrotic liver tissue is characterized by a higher stiffness as compared to healthy liver tissue [112]. The elastic modulus of the depicted fibrotic liver is - with an average of 28 kPa - almost 5 times higher than the one measured in a healthy liver.

In comparison to the above-mentioned US elastography techniques, in which transient elastography in obese patients is compromised, MRE has been shown to have superior diagnostic performance not only for the detection of advanced fibrosis, but also for differentiating the individual progression states from simple steatosis to steatohepatitis [61, 113, 114]. In a recent prospective trial, MRE was found to be more accurate in identifying liver fibrosis (stage 1 or higher) than TE in patients with non-alcoholic fatty liver disease [115]. In this context, Chen and co-workers investigated the precision of MRE for discriminating patients with simple steatosis, steatohepatitis and hepatic fibrosis. A clear difference in hepatic stiffness manifested in all three conditions, and the highest stiffness was observed in patients with hepatic fibrosis (Fig. 4F) followed by steatohepatitis and simple steatosis (Fig. 4E) [116]. These results indicate that the use of MRE allows for separating patients with simple steatosis from the ones with steatohepatitis, which would allow for earlier and more specific therapeutic interventions. The MRE procedure can be incorporated into a routine liver MRI protocol with only a few minutes added to the total scan time [117]. The post-processing procedure is simple, but the hardware and software additions to the MRI are expensive and might impede clinical translation and implementation [118]. Recently, the feasibility of a cost-effective and portable photoacoustic imaging system (PAI) and US dual-modality imaging setup has been evaluated in a preclinical CCl_4-induced murine fibrosis model and it turned out to be an interesting addition to the currently available elastography techniques [11]. This alternative set-up relies on hemoglobin as a chromophore that absorbs light and the combination with US for proper selection of the liver region to be evaluated [119]. The PAI signal is increased in fibrotic livers due to the more heterogeneous tissue structure caused by ECM deposition and angiogenesis. Analogously, PAI has recently also gained interest for application in several other fibrosis-related diseases, including Crohn’s disease [120, 121].

Moreover, a number of tools and technologies have been proposed for molecular imaging of liver fibrosis. These include MRI and nuclear imaging techniques that are used in combination with targeted contrast agents. The liver-specific contrast agent gadolinium ethoxybenzyl dimeglumine (Gd-EOB-DTPA), also known as Primovist® in Europe or Eovist® in the USA, is a MRI contrast agent that was originally developed for the detection of liver metastasis and HCC [122, 123]. After intravenous injection Gd-EOB-DTPA progressively distributes into the hepatocytes via the organic anion transporter polypeptides OATP1B1 and OATP1B3 and excretes into the bile ducts via the multidrug resistance protein 2 (MRP2) [124]. The uptake and excretion of Gd-EOB-DTPA by the hepatocytes is also impaired in liver fibrosis, which enables the detection of severe fibrosis and cirrhosis in patients [125].

Molecular MRI has also shown promise in case of imaging of ECM components, such as elastin and collagen. Evidence for the use of ECM-targeted MR contrast media has been obtained in several liver fibrosis animal models. In this context, we have investigated elastin

Europe PMC Funders Author Manuscripts

Europe PMC Funders Author Manuscripts

as a target for molecular MRI. As exemplified by Fig. 4G-H, a significantly higher contrast enhancement in the perivascular regions in CCl_4-treated fibrotic mice was observed as compared to healthy mice upon the administration of the Gd-containing elastin specific contrast agent ESMA [126]. Similarly, Farrar and colleagues demonstrated that the Gd-containing collagen I-specific contrast agent EP-3533 not only allowed for staging of liver fibrosis via 3D molecular MRI, but also enabled accurate therapy monitoring in mouse and rat models [39, 127, 128].

Besides MRI, also radionuclide-based imaging techniques such as SPECT and PET have been used for molecular imaging of liver fibrosis in preclinical setups. In case of SPECT, Li and colleagues reported on the use of ^{99m}Tc-labeled cyclic RGD penta-peptide for imaging hepatic stellate cells (HSC) in fibrotic rats [129]. The RGD peptide is known to have a high binding affinity to $\alpha_v\beta_3$ integrins, which are upregulated in hepatic fibrosis [130, 131]. Specifically, it was shown that the expression levels of $\alpha_v\beta_3$ integrins on HSC correlate with fibrosis stage, and that non-invasive SPECT-based staging of liver fibrosis is possible with ^{99m}Tc-labeled cRGD [129]. In line with this, PET in combination with CT has been used for the imaging of translocator protein (TSPO) expression in progressive liver fibrosis. The TSPO is a convenient biomarker since it is mainly expressed by macrophages and HSC. The accumulation of the TSPO specific radiotracer ^{18}F-FEDAC correlated well with the severity of liver damage in rats exposed to CCl_4 (Fig. 4I-J) [132].

In summary, significant progress has been made at the clinical level in anatomical and functional imaging of liver fibrosis. However, the abovementioned techniques and protocols entail multiple disadvantages and they do not really permit accurate fibrosis staging and treatment monitoring. At the preclinical level, molecular imaging of liver fibrosis via MRI, PET and SPECT has hinted towards more specific detection of changes in biomarker levels that correlate with disease progression and/or treatment responses, indicating that such probes and protocols may start impacting the diagnosis and treatment of liver fibrosis in the clinic in the near to distant future.

3.3 Kidney fibrosis

Several anatomical and functional imaging techniques, which originate either from standard clinical procedures to categorize a patient with abnormal kidney function or from the assessment of fibrosis in other organs, have been adapted over the years to monitor kidney fibrosis. In the case of anatomical imaging, techniques have focused on abnormalities in the urinary tract as well as in the renal vasculature. Imaging techniques relying on the morphology of the urinary tract include urography and US. Urography is typically performed by intravenously administering a radiopaque contrast agent and by subsequently capturing x-ray images at specific time intervals, thereby allowing for the visualization of abnormalities in the urinary system. Fig. 5A-B exemplify the use of intravenous urography. The kidney in Fig. 5B clearly shows retention of the radiopaque contrast agent in the renal pelvis, as exemplified by the high x-ray contrast and by the deformed and enlarged pelvis and ureter. However, intravenous urography is rarely performed anymore and has been replaced by other imaging modalities, such as CT and MRI [133]. The reasons for this are that CT, on the one hand, provides superior diagnostic sensitivity and a much more

Europe PMC Funders Author Manuscripts

Europe PMC Funders Author Manuscripts

comprehensive examination of the urinary tract and that MRI, on the other hand, allows for repeated examination of urinary tract (due to its radiation-free nature) and for the assessment of additional functional information. Also CT and MRI urography methods, however, have drawbacks, including the somewhat higher radiation dose exposition in CT (as compared to urography), and the lower diagnostic sensitivity for urolithiasis and renal carcinomas and the significantly longer scanning times in MRI [134].

Anatomical US imaging is a standard and broadly applied method for monitoring renal diseases, as it allows for the easy bedside assessment of renal location, contour and size. In case of urinary tract obstruction, the urine efflux clearly manifests in hypoechogenic regions in B-mode US scans (Fig. 5D). However, conventional B-mode US imaging suffers from high operator-dependency, lack of acoustic window and severe scanning limitations in obese patients [19]. These limitations of anatomical imaging have triggered the development of more advanced functional imaging techniques. In the case of functional US imaging, these include elastography, ultrasensitive Doppler US and Superb Microvascular US Imaging (SMI) [135]. Elastography is an emerging imaging technique which evaluates the mechanical properties (i.e. stiffness) of the kidney by inducing a distortion in the tissue and monitoring the subsequent deformation by means of US. Several types of US elastography have been evaluated for their usefulness in imaging renal fibrosis. These encompass quasi-static US elastography, transient US elastography, acoustic radiation force impulse imaging (ARFI), shear wave elasticity imaging (SWEI) and supersonic shear imaging (SSI) [136].

The usefulness of SSI-based US for monitoring kidney function was evaluated by Derieppe and colleagues in a rat model of glomerulosclerosis. The authors observed a significant increase in cortical stiffness as a function of renal dysfunction [137]. However, such US elastography-based techniques impose problems as kidney stiffness may also be affected by anisotropy, vascularization, external pressure, perfusion and the deep location of kidney within the body [137, 138]. In order to overcome problems associated with US elastography and improve the detection of renal vascular disorders, ultrasensitive Doppler US and SMI have been developed. Ultrasensitive Doppler US, contrary to conventional Doppler US, relies on the transmission of tilted plane waves, and the resulting backscattered waves are summed up to produce high resolution images for improved detection of renal blood flow [139]. Several Doppler US parameters such as peak systolic velocity, end diastolic velocity, vascular resistance and vascular compliance have been used as hemodynamic indicators of renal fibrosis. An example of this is shown in Fig. 5E-F, in which significant decrease in cortical vascularity and a reduction in renal blood flow velocities are observed in patients suffering from lupus nephritis with renal cortical fibrosis as compared to healthy volunteers [135, 140]. In addition to ultrasensitive Doppler US, contrast- and non-contrast enhanced SMI, which rely on algorithms to differentiate slow blood flow signals from high background noise, have enabled improved assessment of microvascular perfusion in superficial organs and tissues, including testis, breast, urinary tract and hepato-gastrointestinal tract, and could in principle be easily transferred to the kidney [141–144].

MRI has also been increasingly employed to identify functional changes in the kidney with high resolution and adequate contrast. The two most promising functional MRI approaches for assessing kidney fibrosis are diffusion-weighted imaging (DWI) and blood oxygen level-

Europe PMC Funders Author Manuscripts

Europe PMC Funders Author Manuscripts

dependent (BOLD)-MRI, obviating the need for gadolinium-based contrast agents which may cause nephrogenic systemic fibrosis (NSF) [145–148]. DWI, which represents the microscopic movement of protons, is based on the combined effect of blood circulation and Brownian motion of water molecules, it measures changes in the microstructure of tissues, and it generally quantified via assessment of the Apparent Diffusion Coefficient (ADC) [149, 150]. Inoue and colleagues employed DWI in patients suffering from CKD, and found significantly lower ADC values in the cortex and medulla in kidneys of CKD patients vs. healthy individuals, as a result of restricted water movement (Fig. 5G-H) [151]. This is in line with a study reported by Zhao et al, who found a significant correlation between renal ADC values and pathological fibrosis scores in a small cohort of patients with different CKD grades [152]. There are also studies, however, which indicate that ADC values might not be specific for kidney fibrosis, but rather reflect overall renal function, indicating the need for further investigations [153].

BOLD-MRI is another interesting functional imaging approach for assessing kidney disease. It can distinguish between diamagnetic oxyhemoglobin and paramagnetic deoxyhemoglobin on the basis of their relative differences in magnetic susceptibility. Inoue et al. employed BOLD-MRI to assess hypoxia, which plays an important role in renal fibrosis and in the progression of CKD [151, 154]. In a CKD patient suffering from glomerulonephritis, significant reductions in the levels of oxygenated hemoglobin in the renal cortex and medulla were observed using T2*-based BOLD-MRI (Fig. 5J), and these levels correlated well with the estimated glomerular filtration rate (which reflects overall kidney function) [151].

The abovementioned imaging techniques have been shown to be able to detect both anatomical and functional changes in fibrotic kidneys. Thus far, however, they have not really turned out to be useful for improving diagnosis, staging and treatment monitoring in patients with renal fibrosis and CKD. To improve the non-invasive assessment of kidney fibrosis, and to provide novel tools and technologies for assessing the efficacy of novel anti-fibrotic and anti-CKD therapies, it therefore seems imperative to develop molecular imaging agents, targeted to histopathologically verified biomarkers on certain kidney cells or within the ECM, which are able sensitively and specifically report of the progressions of renal fibrosis and CKD.

3.4 Lung fibrosis

Anatomical imaging of pulmonary fibrosis provides useful information on the delineation and morphological characteristics of fibrous lung tissue. In this context, both radiation-based and radiation-free imaging modalities have been employed (Fig. 6A-F). Radiation-based imaging modalities such as x-ray and CT, which are based on the visualization of (electron-) dense tissues, are used to assess typical characteristics of the diseased lung, such as interstitial patterns, bronchial thickness, pleural effusion, calcification and opacification. As an example, in Fig. 6A-B, a typical chest radiograph of a fibrotic lung shows a reticular opacification as well as a decreased lung volume as compared to a healthy lung [156]. Planar x-ray radiography has long been used as a first basic diagnostic test because of its acquisition speed, high availability, low cost and relatively low exposure to ionizing

Europe PMC Funders Author Manuscripts

Europe PMC Funders Author Manuscripts

radiation (as compared to CT). Over time, however, high-resolution computed tomography (HRCT) imaging has gradually become the method of choice for the diagnosis, staging and surveillance of lung fibrosis, because it provides more detailed anatomical information. As shown in Fig. 6C-D, HRCT scans are able to delineate dilated and thickened respiratory bronchioles with cystic air spaces (also referred to as honeycomb) along with opacification, nodules and decreased lung volume [157–159]. HRCT has also been shown to be superior to standard pulmonary function tests for early disease detection and for monitoring disease progression [160].

Radiation-free imaging modalities such as MRI, which enables 3D pulmonary angiography, have recently emerged as a powerful tool to visualize and distinguish blood vessels in healthy and fibrotic lungs. An example of a 3D MR angiography scan is provided in Fig. 6E-F, depicting a fibrotic lung which is characterized by enlarged, irregularly shaped, inflamed and mucous lined airways blocking the majority of the vessels, while the healthy lung clearly shows well-defined vessels with smooth margins [161, 162].

In recent years, besides anatomical imaging, also functional imaging has been increasingly employed to asses pulmonary fibrosis [163]. In this context, MRI is the most widely used imaging modality [162, 164]. However, traditional proton MRI of the lungs has several drawbacks including respiratory motion, unusually small T2* values and a relatively low water density (which accounts for only 10-25%) [165]. To overcome these limitations, a variety of stronger gradient systems, multichannel coils and parallel imaging techniques have been developed to accelerate and improve MRI acquisition [166]. Lung MRI has also profited from the use of inhaled contrast agents, such as hyperpolarized noble gases, molecular oxygen and fluorinated gases. Gas ventilation MRI has been widely used to image airways, airspaces and allows for the longitudinal quantification of subtle changes in gas exchange, ventilation and alveolar microstructures [167, 168]. In this regard, Walkup and colleagues assessed the feasibility of hyperpolarized ^{129}Xe as an inhaled contrast agent for MRI-based monitoring of the lungs in healthy controls and in patients with cystic fibrosis. A homogeneous ventilation pattern was observed in healthy volunteers (Fig. 6G), whereas in case of patients with cystic fibrosis, relatively inhomogeneous ventilation patterns were detected along with a complete lack of ventilation in a few areas of the lung (Fig. 6H) [167]. While these results are convincing, the high costs of the procedure and the limited availability of useful gases have restricted the use of ventilation MRI to a few expert centers [169, 170].

Recently, self-gated non-contrast-enhanced functional lung (SENCEFUL) MRI has emerged as an interesting and powerful tool for the quantification of lung ventilation, as it does not require contrast agent administration and as it does not require patients to hold their breath [171]. SENCEFUL MRI enables site-resolved ventilation imaging that is improved in spatial resolution, that has fewer artifacts and that is less stressful for patients with lung disease. In order to appraise the clinical feasibility of SENCEFUL MRI, Veldhoen and co-workers performed quantitative ventilation imaging in patients suffering from cystic fibrosis, and reported a significant decline in quantitative ventilation values per respiratory cycle of the whole lungs for patients with cystic fibrosis as compared to healthy volunteers (Fig. 6I-J) [172]. The ventilation map of the fibrotic lungs in Fig. 6J shows a widely distributed pattern

Europe PMC Funders Author Manuscripts

Europe PMC Funders Author Manuscripts

of ventilation deficits which account here for 40% of the whole map area. Further evaluation of the longitudinal observation possibilities and the prognostic value provided by SENCEFUL MRI will aim to confirm these findings and demonstrate the added value of this elegant contrast-agent-free imaging technique.

To extend the above anatomical and functional imaging information, PET-CT has recently emerged as a molecular imaging modality for both indirect and direct monitoring of lung fibrosis. In the case of inflammation, for instance, there is a heightened glycolysis of immune cells, which leads to enhanced uptake of the radioactive glucose analogue ^{18}F-fluoro-deoxyglucose (FDG), which is commonly applied as an inflammation marker in PET imaging [17]. FDG is mostly employed in oncology, but its use has recently been expanded towards the imaging of inflammatory responses. In case of lung fibrosis, FDG uptake is observed in macrophages [173], neutrophils [174] and eosinophils [175], and inflammation imaging can be employed as an indirect means to monitor fibrosis.

A more direct way to perform molecular imaging of lung fibrosis is by targeting integrins. This possibility has been investigated by Mirsadraee and colleagues, who employed ^{18}F-Fluciclatide as a PET contrast agent. Fluciclatide is an arginine-glycine-aspartic acid peptide that binds with high affinity to the integrins $\alpha_v\beta_3$ and $\alpha_v\beta_5$, which are overexpressed on endothelial cells and myofibroblasts in a number of pathological conditions, including fibrosis and cancer [176]. The authors reported a significantly higher uptake of ^{18}F-Fluciclatide in the lungs of patients with lung fibrosis as compared to healthy volunteers. Since the overexpression of integrins plays an important role in the differentiation of fibroblasts into endothelial cells and myofibroblasts, this technique may hold potential for visualizing and quantifying early fibroblast differentiation in pulmonary fibrosis [17].

Another interesting molecular imaging agent is the collagen-targeted PET probe ^{68}Ga-CBP8, which is an analogue of the abovementioned MRI probe EP-3533 [39, 177, 178], and which has recently been successfully tested in a bleomycin-induced mouse model of pulmonary fibrosis [179]. ^{68}Ga-CBP8 showed high specificity for pulmonary fibrosis and high target-to-background ratios in diseased mice, as exemplified by Fig. 6L. Conversely, in the lungs of healthy control mice, PET-CT scans did not show uptake (Fig. 6K). These findings were validated in a second mouse model and in lung tissue obtained from IPF patients, together indicating that ^{68}Ga-CBP8 is a promising candidate for molecular imaging of lung fibrosis.

Taken together, significant progress has been made in non-invasively imaging lung fibrosis. The presented techniques hold several advantages over biopsies and standard clinical tests (including x-ray-based fibrosis imaging). It is therefore expected that in the near future, advanced CT-, MRI- and PET-based techniques, as well as hybrid PET-CT- and PET-MRI-based imaging approaches, will be increasingly employed to perform accurate staging and treatment monitoring of lung fibrosis.

Europe PMC Funders Author Manuscripts

Europe PMC Funders Author Manuscripts

3.5 Heart fibrosis

The medical and technological advancements in the last couple of years have opened up a wide range of possibilities to non-invasively monitor morphological, functional and molecular aspects of cardiac fibrosis [181, 182].

Traditionally anatomical x-ray based contrast luminography has been the gold standard for diagnosing peripheral and coronary arterial disease. This minimally invasive angiography technique is commonly performed by intravenously injecting a radiopaque contrast agent via a catheter in combination with x-ray image acquisition to check for occlusions that cause ischemic cardiomyopathy. This technique is exemplified in Fig. 7A-B in which the upper panel shows normal perfusion, while the bottom panel clearly depicts significant narrowing of the coronary artery lumen [183]. The contrast luminography scans demonstrate the extent and the localization of the obstruction. Hereby, however, no information about functional impairments or the extent of cardiac fibrosis can be obtained, making further diagnostic assessment inevitable.

Alternative imaging approaches, which provide more detailed information on cardiac morphology with higher temporal and spatial resolution are 2D echocardiography, cardiovascular magnetic resonance imaging (CMR) and cardiac CT [182]. Cine CMR is especially useful for the identification of ventricular changes. The applied sequences image the whole heart within a reasonable amount of time, but require breath-holding and electrocardiographically gating to achieve sharp contrast between the bright blood pool and the darker myocardium (Fig. 7C-D) [184]. The acquired images allow wall thickness measurements and determination of ventricular volumes [185]. The expanded ventricular septum in Fig. 7D indicates hypertrophic cardiomyopathy. In order to differentiate cardiomyopathies subtypes more precisely, additional information including contractile function, inflammation as well as fibrosis pattern and location are required.

Most of the imaging data on the functional assessment of myocardial fibrosis is based on CMR imaging and echocardiography [186]. The use of gadolinium-based contrast agents can add another dimension to CMR, via assessment of distribution patterns and kinetics. Here, the 2 major CMR techniques are late gadolinium enhancement (LGE) imaging (Fig. 7E-F) and analysis of the extracellular volume fraction (ECV; see below and Fig. 7G-H). The LGE sequence was first described in 1999 and is based on gadolinium distribution differences in normal and scar tissue, enabling the identification of areas with replacement fibrosis [187]. Typically, the wash-out of gadolinium based contrast agents from the myocardium takes place at 10-20 minutes after intravenous administration. The gadolinium chelates do not cross the cell membranes and accumulate in the extracellular space. In myocardial replacement fibrosis, the extracellular matrix is significantly expanded, which increases the space for contrast agent penetration and which delays wash-out of gadolinium chelates [188]. This prominent accumulation of gadolinium chelates in fibrotic lesions in the heart results in extremely shortened T1 relaxation times, as depicted in Fig 7H, showing an example of transmural replacement fibrosis [189]. In such MRI setups, an inversion pulse is applied to null the signal from the myocardium and/or a phase-sensitive inversion recovery technique is employed to provide appropriate contrast-to-noise ratios [190]. When selecting a proper inversion time, the normal myocardium will appear dark (low signal intensity) and

areas containing gadolinium-based contrast agents will be bright (high signal intensity). This procedure is a potential source for errors and makes comparisons with unaffected myocardium essential, which are difficult to implement in routine clinical practice, because of the heterogeneity of this pathology [188]. Furthermore, although LGE is clinically accepted for the identification of ischemic scars, it is not sensitive enough for accurately assessing diffuse myocardial fibrosis [18].

For the assessment of diffuse cardiac fibrosis, ECV analysis is very suitable. The calculation of the extracellular volume fraction is based on the comparison of native and post-contrast T1 values of the myocardium and the blood [191, 192]. The fibrotic heart tissue in Fig. 7H is represented by higher ECV values in the T1 map than the healthy heart tissue in Fig. 7G [189]. The elevated ECV values reflect the dilated extracellular space in which more contrast agent can accumulate [193]. ECV measurements, based on the MRI-based assessment of the extracellular space, corresponded closely with the histological collagen volume fraction in patients with a mixture of pathologies including ischemic and dilated hypertrophic cardiomyopathy [194, 195]. In the near future, these ECV-based analyses may be applied in cardiac CT as well [196].

Echocardiography has traditionally played a pre-eminent role in the diagnosis, staging and monitoring of cardiomyopathies [197]. The structure of the heart can be easily assessed using US, including ventricular cavity size and wall thicknesses [184]. In addition to 2D and 3D anatomical imaging methods, Doppler echocardiography enables velocity measurements of cardiac motion during the whole cardiac cycle [198]. Changes in the equilibrium of systolic and diastolic flow are important characteristics, for example, for distinguishing restrictive cardiomyopathy from constrictive pericarditis [199]. Speckle tracking echocardiography enables the measurement of the myocardial strain and strain rate, which indicates deformation of the myocardium [200]. This technology identifies and tracks naturally occurring acoustic reflections (speckles). The speckle pattern serves as a fingerprint that is tracked in each frame, independent of angulation and motion [201]. In patients suffering from cardiac fibrosis, the amount of myocardial wall deformation is reduced due to hyperkinesia, caused by the higher tissue stiffness which in turn results in reduced strain values [202]. Several studies have already shown strain reduction via US speckle tracking, similar to the longitudinal and radial examples in Fig. 7I-L [198], and the obtained imaging information accurately predicted the outcomes [203, 204]. Overall, echocardiography and especially US speckle tracking are useful alternatives for cardiac MRI, especially in case of patients with impaired kidney function, which are at risk of developing nephrogenic systemic fibrosis due to exposition to gadolinium-containing contrast agents.

Molecular imaging has shown its usefulness for non-invasive assessment of cardiac fibrosis at both the cellular and the molecular level. In this regard, PET imaging has been extensively employed in combination with CT and MRI to quantify inflammation. The isotopes used for PET tracer have typically a short half-life, and the use of $H_2{}^{15}O$ and $C^{15}O$ as tracers has been evaluated for the quantification of functional parameters, such as cardiac perfusion [205]. Accordingly, cardiac fibrosis can be assessed via the perfusable tissue index (PTI); as fibrotic myocardial tissue is unable to rapidly exchange water molecules, a reduction in PTI

Europe PMC Funders Author Manuscripts
Europe PMC Funders Author Manuscripts

Europe PMC Funders Author Manuscripts

Europe PMC Funders Author Manuscripts

serves as a relatively accurate indicator of fibrosis [206]. While PTI is not yet properly validated against biopsies, it is reduced in advanced dilated cardiomyopathy and after myocardial infarction, and evidence has also been obtained showing a correlation between PTI and compromised contractile function [207]. Other PET-based approaches, involving established molecular imaging agents employed in oncology, are based on the use of ^{68}Ga-DOTATATE for targeting to the somatostatin receptor [208], on ^{11}C-PK11195 which is directed against translocator proteins [209], and on ^{18}F-FMCH [210] and ^{11}C-choline [211] as reporters for membrane formation and lipid metabolism. These probes may be useful for monitoring myocardial inflammation and fibrosis, as they can overcome the nonspecific cardiac uptake that is typically observed for ^{18}F-FDG, which aims to provide imaging information on the activity of infiltrated inflammatory cells (most prominently macrophages) in heart [212].

Apart from imaging infiltrating inflammatory cells, the monitoring of markers involved in cellular and molecular events underlying the pathogenesis of cardiac fibrosis and/or of highly abundant ECM components, such as integrins [213, 214], angiotensin converting enzyme [215], tissue transglutaminase [216], elastin [217], collagen [218–220], fibrin [221] and matrix metalloproteinases (MMP) [222, 223], may also provide useful information for the diagnosis and staging of cardiac fibrosis [224]. An exemplary study in this regard was published by Ziegler and colleagues, who investigated the use of $scFv_{anti\text{-}GP2b/3a}$-^{64}CuMeCOSar, a targeted PET tracer which binds with high affinity to the activated platelet integrin, for molecular imaging of myocardial ischemia [214]. This radiotracer is composed of a single-chain antibody binding to activated integrin $\alpha_{2b}\beta_3$ and a bifunctional sarcophagine chelator which forms a highly stable complex with ^{64}Cu [225]. Platelets are known to contribute to early processes in myocardial ischemia and their location in the heart has been shown to correlate with ischemic area. The integrin glycoprotein receptor GP2b/3a is exclusively expressed and highly abundant on platelets, and it undergoes a confirmational change upon platelet activation [226]. PET-CT scans showed no accumulation of $scFv_{anti\text{-}GP2b/3a}$-^{64}CuMeCOSar in sham-operated mice (Fig. 7M), whereas in ischemic mice, the uptake of this probe in the myocardium was strongly increased (Fig. 7N). This elegant strategy, which employs activated platelets as molecular imaging targets, holds potential to detect and image even low degrees of cardiac ischemia [214].

Myocardial fibrosis is a complex process with an enormous verity of ECM components which are involved, and imaging may provide important means to assess fibrosis accurately and non-invasively. While LGE evaluation remains a common standard, speckle tracking echocardiography and ECV analyses hold promise as functional imaging modalities, especially in case of interstitial fibrosis. Molecular imaging approaches, targeting specific biomarkers such as integrins, platelets, collagen, elastin and MMPs, may assist in the diagnosis, staging and treatment monitoring of cardiac fibrosis in the near to distant future.

3.6 Cancer

Desmoplasia is a stromal reaction in the process of tumor formation and it is a prominent feature of fibrotic tumors. It is characterized by the proliferation of cancer-associated

Europe PMC Funders Author Manuscripts

Europe PMC Funders Author Manuscripts

fibroblasts (CAF), by inflammatory cell infiltration, by endothelial cell alterations and by extensive deposition of ECM molecules. Desmoplasia typically correlates with poor prognosis and with sub-optimal treatment responses, and it is frequently observed in breast, prostate and pancreatic cancer [230]. In this section, we highlight some of the progress made in imaging desmoplastic tumors. We will not focus on fibrogenic and fibrohistiocytic tumors [231], osteosarcoma [232], mesothelioma [233] and fibrous dysplasia [234], which are also classically considered as stromal tumors, because these lesions are relatively rare [235] and because standard morphological imaging techniques, such as x-ray radiography, CT and MRI suffice for proper disease diagnosis and staging.

Thus far, only a relatively small number of diagnostic methods have been evaluated and established for imaging fibrotic tumor stroma. In most of these cases, anatomical and functional imaging techniques are employed. For instance, x-ray examinations of the breast, commonly referred to as mammography, are routinely implemented in the clinic for the detection of fibrotic breast tissue. In mammography scans, low-doses of x-rays are applied to identify potential sites of malignancy. An example of this is provided in Fig. 8A-B, which clearly shows a strong absorption of x-rays in the case of a breast cancer patient as the result of calcifications and fibrous tissue [236].

The diagnosis of other desmoplastic tumors, such as gastrointestinal stromal tumors, pancreatic cancer and prostate cancer, is generally performed using CT or MRI. The anatomical identification of such tumors often is straightforward using these imaging modalities, as the shape and contrast of cancerous lesions tend to be very different from the healthy parts of the organ [237]. In the case of prostate cancer, for instance, the peripheral zone of the prostate is typically characterized by lower signal intensities T2-weighted MRI scans, due to their desmoplastic nature and the presence of calcifications (Fig. 8C-D) [238]. The identification of fibrotic tumors becomes complicated if the tumor is located within a fibrous organ or tissue, and in case of contrast-enhanced scans if tumor perfusion is hindered [239]. A typical example of this is pancreatic cancer, in which fibrosis of the tumor and/or of the surrounding non-malignant parts of the pancreas strongly influences which imaging technique can be employed and which surgical decisions have to be made in terms of intraoperative tumor border definition and resection strategy [240].

When it comes to the assessment of tumor fibrosis, the conventional anatomical techniques discussed above suffer from several shortcomings. Modalities which are able to capture functional information, related e.g. to elastic properties and tissue stiffness, may provide more useful (i.e. more conclusive and more robust) information for determining the degree of tumor fibrosis [241, 242]. In this context, the application of quantitative 2D and 3D shear wave elastography (SWE) has recently been shown to improve the diagnostic performance of B-mode US imaging, enabling the differentiation between benign masses and fibrotic breast cancer lesions [243, 244]. This is exemplified in Fig. 8E-F, showing significantly increased tissue stiffness in case of a fibrotic breast tumor in the 2D color-coded elasticity maps [244]. Elastography values have also been shown to correlate with fibrotic grade and with the severity of breast cancer [245]. If robust and consistent SWE scanning protocols would become broadly available for the assessment of breast masses, this technique will be very valuable for non-invasive cancer diagnosis.

Europe PMC Funders Author Manuscripts

Europe PMC Funders Author Manuscripts

Dynamic contrast-enhanced MRI also allows for the functional assessment of tumor fibrosis. Farace and colleagues, for instance, visualized and quantified MRI contrast enhancement upon injection of the gadolinium-containing and albumin-binding contrast agent MS-325 (i.e. gadofosveset trisodium; Vasovist®) [246] in two different mouse tumor models, which have a distinctly different stromal composition (i.e. BxPC-3 pancreatic carcinoma and DU-145 prostate carcinoma). The authors showed that MS-325 outperforms the standard MRI contrast agent Gd-DTPA by producing high early MRI enhancement during dynamic scans in BxPC-3, i.e. the tumor type with more stroma (Fig. 8G-H), and accumulates mainly in areas of high stromal content [247]. In later scanning phases, the enhancement differences were obscured by the faster washout that was observed in BxPC-3 tumors as compared to DU-145 tumors. In the former model, most of the tumor mass consists of stroma, which together with the relatively high blood vessel density in this tumor (especially within the stromal compartments) explains the rapid and strong enhancement and subsequent washout. Interestingly, these observations are in contrast with results on ^{18}F-FDG PET imaging obtained in a previous study by the same research team [248]. For tumors with a high content of desmoplastic stroma, the detection by ^{18}F-FDG PET appeared less sensitive, due to the more aerobic metabolism with low glucose consumption, which led to an underestimation of the lesion volume when delineating tumor margins. Therefore, DCE-MRI scans with MS-325 are useful to complement ^{18}F-FDG PET imaging and are considered to be very valuable for stromal tumor characterization.

In terms of anticancer drug therapy, desmoplasia and the dense stroma in fibrotic tumors are widely recognized as barriers (and increasingly also as targets) for efficient therapeutic interventions [34, 249–251]. This is in contrast with the field of cancer diagnosis and imaging, in which fibrosis has not yet played a major role. Only a few imaging modalities (x-ray, MRI and US) have been employed to assess tumor fibrosis, and they have thus far only focused on anatomical and functional information. Considering the dynamic changes which are continuously going on in tumor stroma at the molecular level, targeted molecular imaging agents which are specific for stromal/fibrotic biomarkers in the tumor microenvironment may hold significant potential, not only for better diagnosis, staging and prognosis prediction, but also for individualizing and improving therapeutic interventions.

4 Future directions

While our knowledge on the mechanisms and molecular pathways that play a role in fibrosis development and progression has tremendously increased in the last couple of years, advances in the clinical management of fibrotic diseases have been relatively modest. Among the reasons for this are the relatively low sensitivity and specificity of the currently available diagnostic options and surrogate endpoints to be employed in clinical trials, and the relative lack of tools and technologies to non-invasively and longitudinally assess fibrosis.

In the future, these issues can potentially be resolved via the identification of sensitive and specific fibrosis biomarkers. These biomarkers should ideally be measurable as easily and as non-invasively as possible, i.e. in large-cohort screening setups initially via liquid biopsies, and in case of suspicion of disease, via robust and easily repeatable imaging techniques. This

Europe PMC Funders Author Manuscripts

Europe PMC Funders Author Manuscripts

would allow for more accurate and more extensive progression monitoring, and it would be highly useful to facilitate the clinical translation of novel therapies, e.g. via patient selection and longitudinal treatment monitoring. Needle-based biopsies will certainly remain to play an important role in the diagnosis of fibrosis, but particularly in case of the latter, i.e. for monitoring of therapeutic responses to novel drugs in clinical trials, the development of probes and protocols for non-invasive imaging would be very valuable.

The US National Institutes of Health working group on Biomarkers and Surrogate Endpoints has defined a biomarker as “a quantitative indicator for a specific biological or pathological process that varies continuously with the course of disease including the monitoring of treatment response” [255, 256]. Ideally, a biomarker is broadly applicable across a variety of populations and can be measured easily, accurately and reproducibly [257]. In the case of fibrosis, the ECM may provide useful options for biomarker identification and imaging, as both the content and the composition of the ECM correlate with disease stage. Thus far, however, apart from the above described efforts to develop imaging probes which specifically recognize collagen and elastin in liver and cardiac fibrosis (including also atherosclerosis) [126, 128, 217, 258, 259], not many systematic studies have been undertaken, and no ECM-targeted molecular imaging agents have entered clinical trials.

Similarities in the characteristics of fibrosis in parenchymal organs, in systemic autoimmune diseases and in desmoplastic cancers have gradually lead to a transition from pure anatomical imaging to more informative functional imaging setups. Continuously progressing insights on cellular and ECM targets, coupled to the development of highly specific molecular imaging agents, will likely expand the diagnostic armamentarium in the near future, creating new possibilities for even more informative staging and treatment monitoring protocols. Another important future direction will be to connect and combine anatomical, functional and molecular imaging, preferably within a single diagnostic session, and to systematically integrate imaging in the various steps of the patient management cycle (Fig. 9). This cycle should ideally integrate information obtained using tissue biopsies, liquid biopsies and imaging procedures, and it may in the future even encompass radiogenomics, in which imaging characteristics are correlated with gene expression profiles. The rational combination of these different options to obtain information on biomarkers will form the basis for more personalized fibrosis diagnosis and treatment protocols, and it is considered to be the key for improved patient management and therapy responses.

Acknowledgements

The authors gratefully acknowledge financial support by the German Research Foundation (DFG SFB/TRR57: Organ fibrosis – From Mechanisms of injury to modulation of disease, BO3755/3-1 and BO3755/6-1), by the German Ministry of Education and Research(BMBF Consortium STOP-FSGS number 01GM1518A) and by the European Research Council (ERC StG 309495:NeoNaNo). Image templates made freely available by Servier Medical Art (http://smart.servier.com) were used for the preparation of the graphical abstract and of several figure panels.

References

1. Wynn T. Cellular and molecular mechanisms of fibrosis. J Pathol. 2008; 214(2):199–210. [PubMed: 18161745]

Europe PMC Funders Author Manuscripts

2. Border W, Noble N. Transforming growth factor beta in tissue fibrosis. N Engl J Med. 1994; 331(19):1286–1292. [PubMed: 7935686]
3. Friedman S, et al. Therapy for fibrotic diseases: nearing the starting line. Sci Transl Med. 2013; 5(167):167sr1. [PubMed: 23303606]
4. Koyama Y, Brenner D. Liver inflammation and fibrosis. J Clin Invest. 2017; 127(1):55–64. [PubMed: 28045404]
5. Murray L. Editorial: The Cell Types of Fibrosis. Front Pharmacol. 2016; 6(311)
6. Friedman S. Clarity and Challenges in Tissue FibrosisInnovative Medicine. Nakao K, Minato N, Uemoto S, editorsSpringer; 187–194.
7. Marcellin P, et al. Regression of cirrhosis during treatment with tenofovir disoproxil fumarate for chronic hepatitis B: a 5-year open-label follow-up study. Lancet. 2013; 381(9865):468–475. [PubMed: 23234725]
8. D'Ambrosio R, et al. A morphometric and immunohistochemical study to assess the benefit of a sustained virological response in hepatitis C virus patients with cirrhosis. Hepatology. 2012; 56(2): 532–543. [PubMed: 22271347]
9. Cox T, Erler J. Molecular pathways: connecting fibrosis and solid tumor metastasis. Clin Cancer Res. 2014; 20(14):3637–3643. [PubMed: 25028505]
10. McDonald L, LaRue A. Hematopoietic stem cell derived carcinoma-associated fibroblasts: a novel origin. Int J Clin Exp Pathol. 2012; 5(9):863–873. [PubMed: 23119103]
11. Berg Pvd, et al. Preclinical detection of liver fibrosis using dual-modality photoacoustic/ultrasound system. Biomed Opt Express. 2016; 7(12):5081–5091. [PubMed: 28018726]
12. Tung J, et al. Tumor mechanics and metabolic dysfunction. Free Radic Biol Med. 2015; 79:269–280. [PubMed: 25532934]
13. Bachem M, et al. Pancreatic carcinoma cells induce fibrosis by stimulating proliferation and matrix synthesis of stellate cells. Gastroenterology. 2005; 128(4):907–921. [PubMed: 15825074]
14. Klinkhammer B, et al. Treatment of Renal Fibrosis-Turning Challenges into Opportunities. Adv Chronic Kidney Dis. 2017; 24(2):117–129. [PubMed: 28284377]
15. Dulai P, et al. Increased risk of mortality by fibrosis stage in nonalcoholic fatty liver disease: Systematic review and meta-analysis. Hepatology. 2017; 65(5):1557–1565. [PubMed: 28130788]
16. Manning D, Afdhal N. Diagnosis and quantitation of fibrosis. Gastroenterology. 2008; 134(6): 1670–1681. [PubMed: 18471546]
17. Chen D, et al. PET imaging approaches for inflammatory lung diseases: Current concepts and future directions. Eur J Radiol. 2017; 86:371–376. [PubMed: 27663638]
18. Jellis C, et al. Assessment of nonischemic myocardial fibrosis. J Am Coll Cardiol. 2010; 56(2):89–97. [PubMed: 20620723]
19. Wymer D. CHAPTER 5 – ImagingComprehensive Clinical Nephrology. (Fourth Edition). 2010. 56–74.
20. Qayyum A, et al. Evaluation of diffuse liver steatosis by ultrasound, computed tomography, and magnetic resonance imaging: which modality is best? Clin Imaging. 2009; 33(2):110–115. [PubMed: 19237053]
21. Canto M, et al. Frequent detection of pancreatic lesions in asymptomatic high-risk individuals. Gastroenterology. 2012; 142(4):796–804. [PubMed: 22245846]
22. Giannico G, Fogo A. Lupus nephritis: is the kidney biopsy currently necessary in the management of lupus nephritis? Clin J Am Soc Nephrol. 2013; 8(1):138–145. [PubMed: 22977215]
23. Farris A, et al. Morphometric and visual evaluation of fibrosis in renal biopsies. J Am Soc Nephrol. 2011; 22(1):176–186. [PubMed: 21115619]
24. Topham P, Chen Y. Renal BiopsyComprehensive Clinical Nephrology. F J, J JR, F J, editorsSaunders; St. Louis: 2010. 75–82.
25. Fryer E, et al. How often do our liver core biopsies reach current definitions of adequacy? J Clin Pathol. 2013; 66(12):1087–1089. [PubMed: 23863218]
26. Popov Y, Schuppan D. Targeting liver fibrosis: strategies for development and validation of antifibrotic therapies. Hepatology. 2009; 50(4):1294–1306. [PubMed: 19711424]
27. Aranow C, Larché M, Isenberg D. Laboratory TestsABC of Rheumatology. A A, editor2010.

Europe PMC Funders Author Manuscripts

28. Gerlag D, Tak P. How useful are synovial biopsies for the diagnosis of rheumatic diseases? Nature Clinical Practice Rheumatology. 2007; 3(5):248–249.
29. Mahadevan D, Hoff DDV. Tumor-stroma interactions in pancreatic ductal adenocarcinoma. Mol Cancer Ther. 2007; 6(4):1186–1197. [PubMed: 17406031]
30. Ueno H, et al. Clinicopathological significance of the 'keloid-like' collagen and myxoid stroma in advanced rectal cancer. Histopathology. 2002; 40(4):327–334. [PubMed: 11943016]
31. Park JH, et al. The relationship between tumour stroma percentage, the tumour microenvironment and survival in patients with primary operable colorectal cancer. Ann Oncol. 2014; 25(3):644–651. [PubMed: 24458470]
32. Park JH, et al. Evaluation of a tumor microenvironment-based prognostic score in primary operable colorectal cancer. Clin Cancer Res. 2015; 21(4):882–888. [PubMed: 25473000]
33. Bijlsma MF, v Laarhoven HW. The conflicting roles of tumor stroma in pancreatic cancer and their contribution to the failure of clinical trials: a systematic review and critical appraisal. Cancer Metastasis Rev. 2015; 34(1):97–114. [PubMed: 25566685]
34. Neesse A, et al. Stromal biology and therapy in pancreatic cancer. Gut. 2011; 60(6):861–868. [PubMed: 20966025]
35. Wang LM, et al. The prognostic role of desmoplastic stroma in pancreatic ductal adenocarcinoma. Oncotarget. 2016; 7(4):4183–4194. [PubMed: 26716653]
36. Ueno H, et al. Histologic categorization of desmoplastic reaction: its relevance to the colorectal cancer microenvironment and prognosis. Ann Surg Oncol. 2015; 22(5):1504–1512. [PubMed: 25395146]
37. Rousselet MC, et al. Sources of variability in histological scoring of chronic viral hepatitis. Hepatology. 2005; 41(2):257–264. [PubMed: 15660389]
38. Myers RP, Fong A, Shaheen AA. Utilization rates, complications and costs of percutaneous liver biopsy: a population-based study including 4275 biopsies. Liver Int. 2008; 28(5):705–712. [PubMed: 18433397]
39. Farrar CT, et al. 3D molecular MR imaging of liver fibrosis and response to rapamycin therapy in a bile duct ligation rat model. J Hepatol. 2015; 63(3):689–696. [PubMed: 26022693]
40. Rotman Y, Sanyal AJ. Current and upcoming pharmacotherapy for non-alcoholic fatty liver disease. Gut. 2017; 66(1):180–190. [PubMed: 27646933]
41. Gerlinger M, et al. Intratumor heterogeneity and branched evolution revealed by multiregion sequencing. N Engl J Med. 2012; 366(10):883–892. [PubMed: 22397650]
42. Robertson EG, Baxter G. Tumour seeding following percutaneous needle biopsy: the real story! Clin Radiol. 2011; 66(11):1007–1014. [PubMed: 21784421]
43. Diaz LAJ, Bardelli A. Liquid biopsies: genotyping circulating tumor DNA. J Clin Oncol. 2014; 32(6):579–586. [PubMed: 24449238]
44. Crowley E, et al. Liquid biopsy: monitoring cancer-genetics in the blood. Nat Rev Clin Oncol. 2013; 10(8):472–484. [PubMed: 23836314]
45. Alix-Panabières C, Pantel K. Clinical Applications of Circulating Tumor Cells and Circulating Tumor DNA as Liquid Biopsy. Cancer Discov. 2016; 6(5):479–491. [PubMed: 26969689]
46. Liver, E.A.f.S.o. and A.L.p.e.E.d. Higado. EASL-ALEH Clinical Practice Guidelines: Non-invasive tests for evaluation of liver disease severity and prognosis. J Hepatol. 2015; 63(1):237–264. [PubMed: 25911335]
47. Xie Q, et al. The performance of enhanced liver fibrosis (ELF) test for the staging of liver fibrosis: a meta-analysis. PLoS One. 2014; 9(4):e92772. [PubMed: 24736610]
48. Shiha G, et al. Asian-Pacific Association for the Study of the Liver (APASL) consensus guidelines on invasive and non-invasive assessment of hepatic fibrosis: a 2016 update. Hepatol Int. 2017; 11(1):1–30.
49. Wong MG, et al. Circulating bone morphogenetic protein-7 and transforming growth factor-β1 are better predictors of renal end points in patients with type 2 diabetes mellitus. Kidney Int. 2013; 83(2):278–284. [PubMed: 23235570]

Europe PMC Funders Author Manuscripts

50. Papasotiriou M, et al. Serum and urine markers of collagen degradation reflect renal fibrosis in experimental kidney diseases. Nephrol Dial Transplant. 2015; 30(7):1112–1121. [PubMed: 25784725]
51. Genovese F, et al. Turnover of type III collagen reflects disease severity and is associated with progression and microinflammation in patients with IgA nephropathy. Nephrol Dial Transplant. 2016; 31(3):472–479. [PubMed: 26311218]
52. Yokoyama A, et al. Prognostic value of circulating KL-6 in idiopathic pulmonary fibrosis. Respirology. 2006; 11(2):164–168. [PubMed: 16548901]
53. Greene KE, et al. Serum surfactant proteins-A and -D as biomarkers in idiopathic pulmonary fibrosis. Eur Respir J. 2002; 19(3):439–446. [PubMed: 11936520]
54. Rosas IO, et al. MMP1 and MMP7 as potential peripheral blood biomarkers in idiopathic pulmonary fibrosis. PLoS Med. 2008; 5(4):e93. [PubMed: 18447576]
55. Jong Sd, et al. Biomarkers of myocardial fibrosis. J Cardiovasc Pharmacol. 2011; 57(5):522–535. [PubMed: 21423029]
56. López B, et al. Circulating Biomarkers of Myocardial Fibrosis: The Need for a Reappraisal. J Am Coll Cardiol. 2015; 65(22):2449–2456. [PubMed: 26046739]
57. Querejeta R, et al. Serum carboxy-terminal propeptide of procollagen type I is a marker of myocardial fibrosis in hypertensive heart disease. Circulation. 2000; 101(14):1729–1735. [PubMed: 10758057]
58. Klappacher G, et al. Measuring extracellular matrix turnover in the serum of patients with idiopathic or ischemic dilated cardiomyopathy and impact on diagnosis and prognosis. Am J Cardiol. 1995; 75(14):913–918. [PubMed: 7733000]
59. Bauersachs J. Regulation of myocardial fibrosis by MicroRNAs. J Cardiovasc Pharmacol. 2010; 56(5):454–459. [PubMed: 20625314]
60. Fang L, et al. Circulating microRNAs as biomarkers for diffuse myocardial fibrosis in patients with hypertrophic cardiomyopathy. J Transl Med. 2015; 13(314)
61. Sangwaiya MJ, et al. Latest developments in the imaging of fibrotic liver disease. Acta Radiol. 2014; 55(7):802–813. [PubMed: 24226293]
62. Genovese F, et al. The extracellular matrix in the kidney: a source of novel non-invasive biomarkers of kidney fibrosis? Fibrogenesis Tissue Repair. 2014; 7(1):4. [PubMed: 24678881]
63. Maddison PJ, Tikly M. Is it a Connective Tissue Disease?ABC of Rheumatology. Adebajo A, editorBlackwell Publishing; 2010.
64. Cooper RG, et al. Paraspinal muscle fibrosis: a specific pathological component in ankylosing spondylitis. Ann Rheum Dis. 1991; 50(11):755–759. [PubMed: 1837705]
65. Taurog JD, Chhabra A, Colbert RA. Ankylosing Spondylitis and Axial Spondyloarthritis. N Engl J Med. 2016; 374(26):2563–2574. [PubMed: 27355535]
66. Grande FD, et al. Magnetic resonance imaging of inflammatory myopathies. Top Magn Reson Imaging. 2011; 22(2):39–43. [PubMed: 22648079]
67. Sieper J, et al. The Assessment of SpondyloArthritis international Society (ASAS) handbook: a guide to assess spondyloarthritis. Ann Rheum Dis. 2009; 68(Suppl 2):ii1–44. [PubMed: 19433414]
68. Chary-Valckenaere I, d'Agostino MA, Loeuille D. Role for imaging studies in ankylosing spondylitis. Joint Bone Spine. 2011; 78(2):138–143. [PubMed: 20851029]
69. Bennett AN, et al. Evaluation of the diagnostic utility of spinal magnetic resonance imaging in axial spondylarthritis. Arthritis Rheum. 2009; 60(5):1331–1341. [PubMed: 19404934]
70. Bennett AN, et al. The evidence for whole-spine MRI in the assessment of axial spondyloarthropathy. Rheumatology (Oxford). 2010; 49(3):426–432. [PubMed: 20064871]
71. D'Agostino MA, et al. Assessment of peripheral enthesitis in the spondylarthropathies by ultrasonography combined with power Doppler: a cross-sectional study. Arthritis Rheum. 2003; 48(2):523–533. [PubMed: 12571863]
72. Tripathi D, Agarwal V. Quantifying synovial inflammation: Emerging imaging techniques. World J Rheumatol. 2014; 4(3):72–79.

Europe PMC Funders Author Manuscripts

73. Boutry N, et al. Early rheumatoid arthritis: a review of MRI and sonographic findings. AJR Am J Roentgenol. 2007; 189(6):1502–1509. [PubMed: 18029892]
74. Porta F, et al. The role of Doppler ultrasound in rheumatic diseases. Rheumatology (Oxford). 2012; 51(6):976–982. [PubMed: 22253027]
75. Szkudlarek M, et al. Power Doppler ultrasonography for assessment of synovitis in the metacarpophalangeal joints of patients with rheumatoid arthritis: a comparison with dynamic magnetic resonance imaging. Arthritis Rheum. 2001; 44(9):2018–2023. [PubMed: 11592362]
76. Foltz V, et al. Power Doppler ultrasound, but not low-field magnetic resonance imaging, predicts relapse and radiographic disease progression in rheumatoid arthritis patients with low levels of disease activity. Arthritis Rheum. 2012; 64(1):67–76. [PubMed: 21904998]
77. Wakefield RJ, et al. Musculoskeletal ultrasound including definitions for ultrasonographic pathology. J Rheumatol. 2005; 32(12):2485–2487. [PubMed: 16331793]
78. Sofka CM. Ultrasound of the hand and wrist. Ultrasound Q. 2014; 30(3):184–192. [PubMed: 25148487]
79. Szkudlarek M, et al. Interobserver agreement in ultrasonography of the finger and toe joints in rheumatoid arthritis. Arthritis Rheum. 2003; 48(4):955–962. [PubMed: 12687537]
80. Ohrndorf S, Backhaus M. Advances in sonographic scoring of rheumatoid arthritis. Ann Rheum Dis. 2013; 72:69–75.
81. Ohrndorf S, et al. Musculoskeletal ultrasound and other imaging modalities in rheumatoid arthritis. Curr Opin Rheumatol. 2013; 25(3):367–374. [PubMed: 23466958]
82. D'Agostino MA, et al. Exploring a new ultrasound score as a clinical predictive tool in patients with rheumatoid arthritis starting abatacept: results from the APPRAISE study. RMD Open. 2016; 2(1):e000237. [PubMed: 27175297]
83. Taljanovic MS, et al. High-Resolution US of Rheumatologic Diseases. Radiographics. 2015; 35(7): 2026–2048. [PubMed: 26562235]
84. Backhaus M, et al. Evaluation of a novel 7-joint ultrasound score in daily rheumatologic practice: a pilot project. Arthritis Rheum. 2009; 61(9):1194–1201. [PubMed: 19714611]
85. Mohajerani P, et al. Spatiotemporal analysis for indocyanine green-aided imaging of rheumatoid arthritis in hand joints. J Biomed Opt. 2013; 18(9):097004. [PubMed: 24045692]
86. Werner SG, et al. Inflammation assessment in patients with arthritis using a novel in vivo fluorescence optical imaging technology. Ann Rheum Dis. 2012; 71(4):504–510. [PubMed: 22388997]
87. Pfeil A, et al. Fluorescence optical imaging as a novel technique for the visualisation of inflammation in patients with systemic sclerosis with Raynaud's phenomenon: a pilot study. Ann Rheum Dis. 2014; 73(6):1279–1280. [PubMed: 24532678]
88. Pfeil A, et al. The Application of Fluorescence Optical Imaging in Systemic Sclerosis. Biomed Res Int. 2015; 2015 658710.
89. Gordon C, Goldman RR. Systemic Lupus Erythematosus and Lupus - like SyndromesABC of Rheumatology. A A, editor2010.
90. Goh YP, Naidoo P, Ngian GS. Imaging of systemic lupus erythematosus. Part I: CNS, cardiovascular, and thoracic manifestations. Clin Radiol. 2013; 68(2):181–191. [PubMed: 22901452]
91. Kovacs JA, Urowitz MB, Gladman DD. Dilemmas in neuropsychiatric lupus. Rheum Dis Clin North Am. 1993; 19(4):795–814. [PubMed: 8265823]
92. Luyendijk J, et al. Neuropsychiatric systemic lupus erythematosus: lessons learned from magnetic resonance imaging. Arthritis Rheum. 2011; 63(3):722–732. [PubMed: 21360502]
93. Bihan DL. Looking into the functional architecture of the brain with diffusion MRI. Nat Rev Neurosci. 2003; 4(6):469–480. [PubMed: 12778119]
94. Beaulieu C. The basis of anisotropic water diffusion in the nervous system - a technical review. NMR Biomed. 2002; 15(7–8):435–455. [PubMed: 12489094]
95. Emmer BJ, et al. Tract-based spatial statistics on diffusion tensor imaging in systemic lupus erythematosus reveals localized involvement of white matter tracts. Arthritis Rheum. 2010; 62(12): 3716–3721. [PubMed: 20722009]

Europe PMC Funders Author Manuscripts

Europe PMC Funders Author Manuscripts

96. Jung RE, et al. White matter correlates of neuropsychological dysfunction in systemic lupus erythematosus. PLoS One. 2012; 7(1):e28373. [PubMed: 22291880]
97. Jung RE, et al. Diffusion tensor imaging in neuropsychiatric systemic lupus erythematosus. BMC Neurol. 2010; 10(65)
98. Zhang L, et al. Diffusion changes in patients with systemic lupus erythematosus. Magn Reson Imaging. 2007; 25(3):399–405. [PubMed: 17371731]
99. Lee SP, et al. Efficacy of magnetic resonance diffusion tensor imaging and three-dimensional fiber tractography in the detection of clinical manifestations of central nervous system lupus. Magn Reson Imaging. 2014; 32(5):598–603. [PubMed: 24629511]
100. Case courtesy of A.Prof Frank Gaillard, Radiopaedia.org, rID: 43359
101. Angulo P, et al. Liver Fibrosis, but No Other Histologic Features, Is Associated With Long-term Outcomes of Patients With Nonalcoholic Fatty Liver Disease. Gastroenterology. 2015; 149(2): 389–397. [PubMed: 25935633]
102. (EASL), E.A.f.t.S.o.t.L., E.A.f.t.S.o.D. (EASD), and E.A.f.t.S.o.O. (EASO). EASL-EASD-EASO Clinical Practice Guidelines for the management of non-alcoholic fatty liver disease. J Hepatol. 2016; 64(6):1388–1402. [PubMed: 27062661]
103. Choong CC, Venkatesh SK, Siew EP. Accuracy of routine clinical ultrasound for staging of liver fibrosis. J Clin Imaging Sci. 2012; 2(58)
104. Smith AD, et al. Liver Surface Nodularity Quantification from Routine CT Images as a Biomarker for Detection and Evaluation of Cirrhosis. Radiology. 2016; 280(3):771–778. [PubMed: 27089026]
105. Beers BEV, Daire JL, Garteiser P. New imaging techniques for liver diseases. J Hepatol. 2015; 62(3):690–700. [PubMed: 25457198]
106. Sandrin L, et al. Transient elastography: a new noninvasive method for assessment of hepatic fibrosis. Ultrasound Med Biol. 2003; 29(12):1705–1713. [PubMed: 14698338]
107. Foucher J, et al. Diagnosis of cirrhosis by transient elastography (FibroScan): a prospective study. Gut. 2006; 55(3):403–408. [PubMed: 16020491]
108. Castera L, Forns X, Alberti A. Non-invasive evaluation of liver fibrosis using transient elastography. J Hepatol. 2008; 48(5):835–847. [PubMed: 18334275]
109. Myers RP, et al. Feasibility and diagnostic performance of the FibroScan XL probe for liver stiffness measurement in overweight and obese patients. Hepatology. 2012; 55(1):199–208. [PubMed: 21898479]
110. Mueller S, Sandrin L. Liver stiffness: a novel parameter for the diagnosis of liver disease. Hepat Med. 2010; 25(2):49–67.
111. Liu J, et al. Liver Shear-Wave Velocity and Serum Fibrosis Markers to Diagnose Hepatic Fibrosis in Patients with Chronic Viral Hepatitis B. Korean J Radiol. 2016; 17(3):396–404. [PubMed: 27134527]
112. Feng YH, et al. Shear wave elastography results correlate with liver fibrosis histology and liver function reserve. World J Gastroenterol. 2016; 22(17):4338–4344. [PubMed: 27158202]
113. Loomba R, et al. Magnetic resonance elastography predicts advanced fibrosis in patients with nonalcoholic fatty liver disease: a prospective study. Hepatology. 2014; 60(6):1920–1928. [PubMed: 25103310]
114. Imajo K, et al. Magnetic Resonance Imaging More Accurately Classifies Steatosis and Fibrosis in Patients With Nonalcoholic Fatty Liver Disease Than Transient Elastography. Gastroenterology. 2016; 150(3):626–637. [PubMed: 26677985]
115. Park CC, et al. Magnetic Resonance Elastography vs Transient Elastography in Detection of Fibrosis and Noninvasive Measurement of Steatosis in Patients With Biopsy-Proven Nonalcoholic Fatty Liver Disease. Gastroenterology. 2017; 152(3):598–607. [PubMed: 27911262]
116. Chen J, et al. Early detection of nonalcoholic steatohepatitis in patients with nonalcoholic fatty liver disease by using MR elastography. Radiology. 2011; 259(3):749–756. [PubMed: 21460032]
117. Venkatesh SK, Yin M, Ehman RL. Magnetic resonance elastography of liver: clinical applications. J Comput Assist Tomogr. 2013; 37(6):887–896. [PubMed: 24270110]

Europe PMC Funders Author Manuscripts

118. Dyvorne HA, et al. Prospective comparison of magnetic resonance imaging to transient elastography and serum markers for liver fibrosis detection. Liver Int. 2016; 36(5):659–666. [PubMed: 26744140]
119. Xu G, et al. The functional pitch of an organ: quantification of tissue texture with photoacoustic spectrum analysis. Radiology. 2014; 271(1):248–254. [PubMed: 24475855]
120. Lei H, et al. Characterizing intestinal inflammation and fibrosis in Crohn's disease by photoacoustic imaging: feasibility study. Biomed Opt Express. 2016; 7(7):2837–2848. [PubMed: 27446710]
121. Knieling F, et al. Multispectral Optoacoustic Tomography for Assessment of Crohn's Disease Activity. N Engl J Med. 2017; 376(13):1292–1294. [PubMed: 28355498]
122. Vogl TJ, et al. Liver tumors: comparison of MR imaging with Gd-EOB-DTPA and Gd-DTPA. Radiology. 1996; 200(1):59–67. [PubMed: 8657946]
123. Hammerstingl R, et al. Diagnostic efficacy of gadoxetic acid (Primovist)-enhanced MRI and spiral CT for a therapeutic strategy: comparison with intraoperative and histopathologic findings in focal liver lesions. Eur Radiol. 2008; 18(3):457–467. [PubMed: 18058107]
124. Beers BEV, P CM, H HK. Primovist, Eovist: what to expect? J Hepatol. 2012; 57(2):421–429. [PubMed: 22504332]
125. Feier D, et al. Liver fibrosis: histopathologic and biochemical influences on diagnostic efficacy of hepatobiliary contrast-enhanced MR imaging in staging. Radiology. 2013; 269(2):460–468. [PubMed: 23878281]
126. Ehling J, et al. Elastin-based molecular MRI of liver fibrosis. Hepatology. 2013; 58(4):1517–1518. [PubMed: 23424008]
127. Polasek M, et al. Molecular MR imaging of liver fibrosis: a feasibility study using rat and mouse models. J Hepatol. 2012; 57(3):549–555. [PubMed: 22634342]
128. Fuchs BC, et al. Molecular MRI of collagen to diagnose and stage liver fibrosis. J Hepatol. 2013; 59(5):992–998. [PubMed: 23838178]
129. Li F, et al. Molecular imaging of hepatic stellate cell activity by visualization of hepatic integrin αvβ3 expression with SPECT in rat. Hepatology. 2011; 54(3):1020–1030. [PubMed: 21618580]
130. Kuijpers BH, et al. Preparation and evaluation of glycosylated arginine-glycine-aspartate (RGD) derivatives for integrin targeting. Bioconjug Chem. 2007; 18(6):1847–1854. [PubMed: 17922547]
131. Patsenker E, et al. Pharmacological inhibition of integrin alphavbeta3 aggravates experimental liver fibrosis and suppresses hepatic angiogenesis. Hepatology. 2009; 50(5):1501–1511. [PubMed: 19725105]
132. Hatori A, et al. Utility of Translocator Protein (18 kDa) as a Molecular Imaging Biomarker to Monitor the Progression of Liver Fibrosis. Sci Rep. 2015; 27(5) 17327.
133. Tublin M, , et al. Diagnostic Imaging: Genitourinary. Third Edition. Philadelphia: Elsevier; 2016.
134. Silverman SG, Leyendecker JR, Amis ESJ. What is the current role of CT urography and MR urography in the evaluation of the urinary tract? Radiology. 2009; 250(2):309–323. [PubMed: 19188307]
135. Correas JM, et al. Ultrasound-based imaging methods of the kidney-recent developments. Kidney Int. 2016; 90(6):1199–1210. [PubMed: 27665116]
136. Gennisson JL, et al. Ultrasound elastography: principles and techniques. Diagn Interv Imaging. 2013; 94(5):487–495. [PubMed: 23619292]
137. Derieppe M, et al. Detection of intrarenal microstructural changes with supersonic shear wave elastography in rats. Eur Radiol. 2012; 22(1):243–250. [PubMed: 21845464]
138. Peride I, et al. Value of ultrasound elastography in the diagnosis of native kidney fibrosis. Med Ultrason. 2016; 18(3):362–369. [PubMed: 27622414]
139. Errico C, et al. Transcranial functional ultrasound imaging of the brain using microbubble-enhanced ultrasensitive Doppler. Neuroimage. 2016; 124(Pt A):752–761. [PubMed: 26416649]
140. Gao J, et al. Correlation between Doppler parameters and renal cortical fibrosis in lupus nephritis: a preliminary observation. Ultrasound Med Biol. 2013; 39(2):275–282. [PubMed: 23245821]

Europe PMC Funders Author Manuscripts

141. Lee YS, et al. Superb microvascular imaging for the detection of parenchymal perfusion in normal and undescended testes in young children. Eur J Radiol. 2016; 85(3):649–656. [PubMed: 26860680]
142. Xiao XY, et al. Superb microvascular imaging in diagnosis of breast lesions: a comparative study with contrast-enhanced ultrasonographic microvascular imaging. Br J Radiol. 2016; 89(1066) 20160546.
143. Kim HK, et al. Feasibility of superb microvascular imaging to detect high-grade vesicoureteral reflux in children with urinary tract infection. Eur Radiol. 2017
144. Ohno Y, Fujimoto T, Shibata Y. A New Era in Diagnostic Ultrasound, Superb Microvascular Imaging: Preliminary Results in Pediatric Hepato-Gastrointestinal Disorders. Eur J Pediatr Surg. 2017; 27(1):20–25. [PubMed: 27699732]
145. Zhang JL, et al. New magnetic resonance imaging methods in nephrology. Kidney Int. 2014; 85(4):768–778. [PubMed: 24067433]
146. Mahmoud H, et al. Imaging the kidney using magnetic resonance techniques: structure to function. Curr Opin Nephrol Hypertens. 2016; 25(6):487–493. [PubMed: 27636770]
147. Grenier N, Merville P, Combe C. Radiologic imaging of the renal parenchyma structure and function. Nat Rev Nephrol. 2016; 12(6):348–359. [PubMed: 27067530]
148. Rogosnitzky M, Branch S. Gadolinium-based contrast agent toxicity: a review of known and proposed mechanisms. Biometals. 2016; 29(3):365–376. [PubMed: 27053146]
149. Eisenberger U, et al. Living renal allograft transplantation: diffusion-weighted MR imaging in longitudinal follow-up of the donated and the remaining kidney. Radiology. 2014; 270(3):800–808. [PubMed: 24475796]
150. Jiang K, et al. Noninvasive Assessment of Renal Fibrosis with Magnetization Transfer MR Imaging: Validation and Evaluation in Murine Renal Artery Stenosis. Radiology. 2016 160566.
151. Inoue T, et al. Noninvasive evaluation of kidney hypoxia and fibrosis using magnetic resonance imaging. J Am Soc Nephrol. 2011; 22(8):1429–1434. [PubMed: 21757771]
152. Zhao J, et al. Assessment of renal fibrosis in chronic kidney disease using diffusion-weighted MRI. Clin Radiol. 2014; 69(11):1117–1122. [PubMed: 25062924]
153. Boor P, et al. Diffusion-weighted MRI does not reflect kidney fibrosis in a rat model of fibrosis. J Magn Reson Imaging. 2015; 42(4):990–998. [PubMed: 25630829]
154. Matsumoto M, et al. Hypoperfusion of peritubular capillaries induces chronic hypoxia before progression of tubulointerstitial injury in a progressive model of rat glomerulonephritis. J Am Soc Nephrol. 2004; 15(6):1574–1581. [PubMed: 15153568]
155. *Case courtesy of Dr Aditya Shetty, Radiopaedia.org, rID: 27633.*
156. Mathieson J, et al. Chronic diffuse infiltrative lung disease: comparison of diagnostic accuracy of CT and chest radiography. Radiology. 1989; 171(1):111–6. [PubMed: 2928513]
157. Kusmirek JE, Martin MD, Kanne JP. Imaging of Idiopathic Pulmonary Fibrosis. Radiol Clin North Am. 2016; 54(6):997–1014. [PubMed: 27719984]
158. Murphy KP, Maher MM, O'Connor OJ. Imaging of Cystic Fibrosis and Pediatric Bronchiectasis. AJR Am J Roentgenol. 2016; 206(3):448–454. [PubMed: 26901001]
159. M S, L DA. Idiopathic pulmonary fibrosis/usual interstitial pneumonia: imaging diagnosis, spectrum of abnormalities, and temporal progression. Proc Am Thorac Soc. 2006; 3(4):307–314. [PubMed: 16738194]
160. Jong PAd, et al. Progressive damage on high resolution computed tomography despite stable lung function in cystic fibrosis. Eur Respir J. 2004; 23(1):93–97. [PubMed: 14738238]
161. Bieri O. Ultra-fast steady state free precession and its application to in vivo (1)H morphological and functional lung imaging at 1.5 tesla. Magn Reson Med. 2013; 70(3):657–663. [PubMed: 23813579]
162. Miller GW, et al. Advances in functional and structural imaging of the human lung using proton MRI. NMR Biomed. 2014; 27(12):1542–1556. [PubMed: 24990096]
163. Wielpütz MO, Eichinger M, Puderbach M. Magnetic resonance imaging of cystic fibrosis lung disease. J Thorac Imaging. 2013; 28(3):151–159. [PubMed: 23545948]

Europe PMC Funders Author Manuscripts

164. Wielpütz MO, Mall MA. Imaging modalities in cystic fibrosis: emerging role of MRI. Curr Opin Pulm Med. 2015; 21(6):609–616. [PubMed: 26390331]
165. Theilmann RJ, et al. Quantitative MRI measurement of lung density must account for the change in T(2) (*) with lung inflation. J Magn Reson Imaging. 2009; 30(3):527–534. [PubMed: 19630079]
166. Wielpütz M, Kauczor HU. MRI of the lung: state of the art. Diagn Interv Radiol. 2012; 18(4): 344–353. [PubMed: 22434450]
167. Walkup LL, et al. Feasibility, tolerability and safety of pediatric hyperpolarized 129Xe magnetic resonance imaging in healthy volunteers and children with cystic fibrosis. Pediatr Radiol. 2016; 46(12):1651–1662. [PubMed: 27492388]
168. Kruger SJ, et al. Functional imaging of the lungs with gas agents. J Magn Reson Imaging. 2016; 43(2):295–315. [PubMed: 26218920]
169. Biederer J, et al. Functional magnetic resonance imaging of the lung. Semin Respir Crit Care Med. 2014; 35(1):74–82. [PubMed: 24481761]
170. Hersman FW, et al. Large production system for hyperpolarized 129Xe for human lung imaging studies. Acad Radiol. 2008; 15(6):683–692. [PubMed: 18486005]
171. Fischer A, et al. SElf-gated Non-Contrast-Enhanced FUnctional Lung imaging (SENCEFUL) using a quasi-random fast low-angle shot (FLASH) sequence and proton MRI. NMR Biomed. 2014; 27(8):907–917. [PubMed: 24820869]
172. Veldhoen S, et al. Self-gated Non-Contrast-enhanced Functional Lung MR Imaging for Quantitative Ventilation Assessment in Patients with Cystic Fibrosis. Radiology. 2016 Oct 6. 160355.
173. Saha D, et al. Micro-autoradiographic assessment of cell types contributing to 2-deoxy-2-[(18)F]fluoro-D-glucose uptake during ventilator-induced and endotoxemic lung injury. Mol Imaging Biol. 2013; 15(1):19–27. [PubMed: 22752654]
174. Schuster DP, et al. Regulation of lipopolysaccharide-induced increases in neutrophil glucose uptake. Am J Physiol Lung Cell Mol Physiol. 2007; 292(4):L845–851. [PubMed: 17122354]
175. Venge P, et al. Mechanisms of basal and cytokine-induced uptake of glucose in normal human eosinophils: relation to apoptosis. Respir Med. 2003; 97(10):1109–1119. [PubMed: 14561018]
176. Kenny LM, et al. Phase I trial of the positron-emitting Arg-Gly-Asp (RGD) peptide radioligand 18F-AH111585 in breast cancer patients. J Nucl Med. 2008; 49(6):879–886. [PubMed: 18483090]
177. Caravan P, et al. Collagen-targeted MRI contrast agent for molecular imaging of fibrosis. Angew Chem Int Ed Engl. 2007; 46(43):8171–8173. [PubMed: 17893943]
178. Caravan P, et al. Molecular magnetic resonance imaging of pulmonary fibrosis in mice. Am J Respir Cell Mol Biol. 2013; 49(6):1120–1126. [PubMed: 23927643]
179. Désogère P, et al. Type I collagen-targeted PET probe for pulmonary fibrosis detection and staging in preclinical models. Sci Transl Med. 2017; 9(384)
180. *Case courtesy of Dr Henry Knipe, Radiopaedia.org, rID: 31525.*
181. Madonna R, et al. "State-of-Art" paper of the Italian Working Group on Atherosclerosis: Preclinical assessment of early coronary atherosclerosis. Int J Cardiol. 2016; 214:442–447. [PubMed: 27093681]
182. Gunaratnam K, et al. Review of cardiomyopathy imaging. Eur J Radiol. 2013; 82(10):1763–1775. [PubMed: 23827801]
183. Patel MC, et al. Have CT and MR Angiography Replaced Catheter Angiography in Diagnosing Peripheral Arterial Disease? J Am Coll Radiol. 2015; 12(9):909–914. [PubMed: 26160043]
184. Nagueh SF, et al. American Society of Echocardiography clinical recommendations for multimodality cardiovascular imaging of patients with hypertrophic cardiomyopathy: Endorsed by the American Society of Nuclear Cardiology, Society for Cardiovascular Magnetic Resonance, and Society of Cardiovascular Computed Tomography. J Am Soc Echocardiogr. 2011; 24(5):473–498. [PubMed: 21514501]
185. Rickers C, et al. Utility of cardiac magnetic resonance imaging in the diagnosis of hypertrophic cardiomyopathy. Circulation. 2005; 112(6):855–861. [PubMed: 16087809]

Europe PMC Funders Author Manuscripts

186. Won S, et al. Noninvasive imaging of myocardial extracellular matrix for assessment of fibrosis. Curr Opin Cardiol. 2013; 28(3):282–289. [PubMed: 23549230]

187. Kim RJ, et al. Relationship of MRI delayed contrast enhancement to irreversible injury, infarct age, and contractile function. Circulation. 1999; 100(9):1992–2002. [PubMed: 10556226]

188. Everett RJ, et al. Assessment of myocardial fibrosis with T1 mapping MRI. Clin Radiol. 2016; 71(8):768–778. [PubMed: 27005015]

189. Rathod RH, Powell AJ, Geva T. Myocardial Fibrosis in Congenital Heart Disease. Circ J. 2016; 80(6):1300–1307. [PubMed: 27170048]

190. Kellman P, et al. Phase-sensitive inversion recovery for detecting myocardial infarction using gadolinium-delayed hyperenhancement. Magn Reson Med. 2002; 47(2):372–383. [PubMed: 11810682]

191. Kellman P, et al. Extracellular volume fraction mapping in the myocardium, part 2: initial clinical experience. J Cardiovasc Magn Reson. 2012; 14(64)

192. Moon JC, et al. Myocardial T1 mapping and extracellular volume quantification: a Society for Cardiovascular Magnetic Resonance (SCMR) and CMR Working Group of the European Society of Cardiology consensus statement. J Cardiovasc Magn Reson. 2013; 15(92)

193. Ugander M, et al. Extracellular volume imaging by magnetic resonance imaging provides insights into overt and sub-clinical myocardial pathology. Eur Heart J. 2012; 33(10):1268–1278. [PubMed: 22279111]

194. Sibley CT, et al. T1 Mapping in cardiomyopathy at cardiac MR: comparison with endomyocardial biopsy. Radiology. 2012; 265(3):724–732. [PubMed: 23091172]

195. Miller CA, et al. Comprehensive validation of cardiovascular magnetic resonance techniques for the assessment of myocardial extracellular volume. Circ Cardiovasc Imaging. 2013; 6(3):373–383. [PubMed: 23553570]

196. Nacif MS, et al. Interstitial myocardial fibrosis assessed as extracellular volume fraction with low-radiation-dose cardiac CT. Radiology. 2012; 264(3):876–883. [PubMed: 22771879]

197. Afonso LC, et al. Echocardiography in hypertrophic cardiomyopathy: the role of conventional and emerging technologies. JACC Cardiovasc Imaging. 2008; 1(6):787–800. [PubMed: 19356516]

198. Nagueh SF, et al. Tissue Doppler imaging consistently detects myocardial abnormalities in patients with hypertrophic cardiomyopathy and provides a novel means for an early diagnosis before and independently of hypertrophy. Circulation. 2001; 104(2):128–130. [PubMed: 11447072]

199. O'Donnell DH, et al. Cardiac MR imaging of nonischemic cardiomyopathies: imaging protocols and spectra of appearances. Radiology. 2012; 262(2):403–422. [PubMed: 22282181]

200. Serri K, et al. Global and regional myocardial function quantification by two-dimensional strain: application in hypertrophic cardiomyopathy. J Am Coll Cardiol. 2006; 47(6):1175–1181. [PubMed: 16545649]

201. Graham-Brown MP, et al. Imaging of Myocardial Fibrosis in Patients with End-Stage Renal Disease: Current Limitations and Future Possibilities. Biomed Res Int. 2017; 2017 5453606.

202. Urheim S, et al. Myocardial strain by Doppler echocardiography. Validation of a new method to quantify regional myocardial function. Circulation. 2000; 102(10):1158–1164. [PubMed: 10973846]

203. Reant P, et al. Global longitudinal strain is associated with heart failure outcomes in hypertrophic cardiomyopathy. Heart. 2016; 102(10):741–747. [PubMed: 26857213]

204. Liu H, et al. Role of Global Longitudinal Strain in Predicting Outcomes in Hypertrophic Cardiomyopathy. Am J Cardiol. 2017 S0002-9149(17)30875-5.

205. Sado DM, Flett AS, Moon JC. Novel imaging techniques for diffuse myocardial fibrosis. Future Cardiol. 2011; 7(5):643–650. [PubMed: 21929344]

206. Gyöngyösi M, et al. Myocardial fibrosis: biomedical research from bench to bedside. Eur J Heart Fail. 2017; 19(2):177–191. [PubMed: 28157267]

207. Knaapen P, et al. Does myocardial fibrosis hinder contractile function and perfusion in idiopathic dilated cardiomyopathy? PET and MR imaging study. Radiology. 2006; 240(2):380–388. [PubMed: 16864667]

Europe PMC Funders Author Manuscripts

Europe PMC Funders Author Manuscripts

208. Li X, et al. Specific somatostatin receptor II expression in arterial plaque: (68)Ga-DOTATATE autoradiographic, immunohistochemical and flow cytometric studies in apoE-deficient mice. Atherosclerosis. 2013; 230(1):33–39. [PubMed: 23958249]
209. Gaemperli O, et al. Imaging intraplaque inflammation in carotid atherosclerosis with 11C-PK11195 positron emission tomography/computed tomography. Eur Heart J. 2012; 33(15):1902–1910. [PubMed: 21933781]
210. Bucerius J, et al. Feasibility of 18F-fluoromethylcholine PET/CT for imaging of vessel wall alterations in humans--first results. Eur J Nucl Med Mol Imaging. 2008; 35(4):815–820. [PubMed: 18183393]
211. Kato K, et al. Evaluation and comparison of 11C-choline uptake and calcification in aortic and common carotid arterial walls with combined PET/CT. Eur J Nucl Med Mol Imaging. 2009; 36(10):1622–1628. [PubMed: 19430785]
212. Tarkin JM, Joshi FR, Rudd JH. PET imaging of inflammation in atherosclerosis. Nat Rev Cardiol. 2014; 11(8):443–457. [PubMed: 24913061]
213. Borne SWvd, et al. Molecular imaging of interstitial alterations in remodeling myocardium after myocardial infarction. J Am Coll Cardiol. 2008; 52(24):2017–2028. [PubMed: 19055994]
214. Ziegler M, et al. Highly Sensitive Detection of Minimal Cardiac Ischemia using Positron Emission Tomography Imaging of Activated Platelets. Sci Rep. 2016; 6 38161.
215. Dilsizian V, et al. Molecular imaging of human ACE-1 expression in transgenic rats. JACC Cardiovasc Imaging. 2012; 5(4):409–418. [PubMed: 22498331]
216. Nahrendorf M, et al. Transglutaminase activity in acute infarcts predicts healing outcome and left ventricular remodelling: implications for FXIII therapy and antithrombin use in myocardial infarction. Eur Heart J. 2008; 29(4):445–454. [PubMed: 18276618]
217. Makowski MR, et al. Assessment of atherosclerotic plaque burden with an elastin-specific magnetic resonance contrast agent. Nat Med. 2011; 17(3):383–388. [PubMed: 21336283]
218. Helm PA, et al. Postinfarction myocardial scarring in mice: molecular MR imaging with use of a collagen-targeting contrast agent. Radiology. 2008; 247(3):788–796. [PubMed: 18403626]
219. Muzard J, et al. Non-invasive molecular imaging of fibrosis using a collagen-targeted peptidomimetic of the platelet collagen receptor glycoprotein VI. PLoS One. 2009; 4(5):e5585. [PubMed: 19440310]
220. Klink A, et al. In vivo characterization of a new abdominal aortic aneurysm mouse model with conventional and molecular magnetic resonance imaging. J Am Coll Cardiol. 2011; 58(24):2522–2530. [PubMed: 22133853]
221. Spuentrup E, et al. MR imaging of thrombi using EP-2104R, a fibrin-specific contrast agent: initial results in patients. Eur Radiol. 2008; 18(9):1995–2005. [PubMed: 18425519]
222. Su H, et al. Noninvasive targeted imaging of matrix metalloproteinase activation in a murine model of postinfarction remodeling. Circulation. 2005; 112(20):3157–3167. [PubMed: 16275862]
223. Sahul ZH, et al. Targeted imaging of the spatial and temporal variation of matrix metalloproteinase activity in a porcine model of postinfarct remodeling: relationship to myocardial dysfunction. Circ Cardiovasc Imaging. 2011; 4(4):381–391. [PubMed: 21505092]
224. Reimann C, et al. Molecular imaging of the extracellular matrix in the context of atherosclerosis. Adv Drug Deliv Rev. 2016 available online.
225. Alt K, et al. Single-chain antibody conjugated to a cage amine chelator and labeled with positron-emitting copper-64 for diagnostic imaging of activated platelets. Mol Pharm. 2014; 11(8):2855–2863. [PubMed: 24999533]
226. Armstrong PC, Peter K. GPIIb/IIIa inhibitors: from bench to bedside and back to bench again. Thromb Haemost. 2012; 107(5):808–814. [PubMed: 22370973]
227. http://www.qmedicine.co.in/top%20health%20topics/A/Angiography-Coronary.html.
228. http://www.nsccheart.com/services/north-shore-cardiology-consultants/interventional-cardiology/.
229. *Case courtesy of Dr Roberto Schubert*, Radiopaedia.org, *rID: 14225*.

Europe PMC Funders Author Manuscripts

230. Bremnes RM, et al. The role of tumor stroma in cancer progression and prognosis: emphasis on carcinoma-associated fibroblasts and non-small cell lung cancer. J Thorac Oncol. 2011; 6(1): 209–217. [PubMed: 21107292]
231. Kang HS, Ahn JM, Kang Y. Oncologic Imaging: Bone Tumors. Vol. 1. Springer; Singapore: 2017.
232. Group EESNW. Bone sarcomas: ESMO Clinical Practice Guidelines for diagnosis, treatment and follow-up. Ann Oncol. 2014; 25(Suppl 3):113–123.
233. Baas P, et al. Malignant pleural mesothelioma: ESMO Clinical Practice Guidelines for diagnosis, treatment and follow-up. Ann Oncol. 2015; 26(Suppl 5):31–39.
234. Bousson V, et al. Fibrous dysplasia and McCune-Albright syndrome: imaging for positive and differential diagnoses, prognosis, and follow-up guidelines. Eur J Radiol. 2014; 83(10):1828–1842. [PubMed: 25043984]
235. Biermann JS, et al. Bone cancer. J Natl Compr Canc Netw. 2013; 11(6):688–723. [PubMed: 23744868]
236. Oeffinger KC, et al. Breast Cancer Screening for Women at Average Risk: 2015 Guideline Update From the American Cancer Society. JAMA. 2015; 314(15):1599–1614. [PubMed: 26501536]
237. Barral M, et al. Gastrointestinal cancers in inflammatory bowel disease: An update with emphasis on imaging findings. Crit Rev Oncol Hematol. 2016; 97:30–46. [PubMed: 26315381]
238. Andrade L, , et al. Multiparametric 3T MR imaging of the prostate - acquisition protocols and image evaluation. ECR 2014; 2014.
239. Erkan M, et al. The role of stroma in pancreatic cancer: diagnostic and therapeutic implications. Nat Rev Gastroenterol Hepatol. 2012; 9(8):454–467. [PubMed: 22710569]
240. Erkan M, et al. How fibrosis influences imaging and surgical decisions in pancreatic cancer. Front Physiol. 2012; 3(389)
241. Cox TR, Erler JT. Remodeling and homeostasis of the extracellular matrix: implications for fibrotic diseases and cancer. Dis Model Mech. 2011; 4(2):165–178. [PubMed: 21324931]
242. Lyshchik A, et al. Thyroid gland tumor diagnosis at US elastography. Radiology. 2005; 237(1): 202–211. [PubMed: 16118150]
243. Barr RG, et al. WFUMB guidelines and recommendations for clinical use of ultrasound elastography: Part 2: breast. Ultrasound Med Biol. 2015; 41(5):1148–1160. [PubMed: 25795620]
244. Tian J, et al. Application of 3D and 2D quantitative shear wave elastography (SWE) to differentiate between benign and malignant breast masses. Sci Rep. 2017; 7 41216.
245. Evans A, et al. Invasive breast cancer: relationship between shear-wave elastographic findings and histologic prognostic factors. Radiology. 2012; 263(3):673–677. [PubMed: 22523322]
246. Shamsi K, Yucel EK, Chamberlin P. A summary of safety of gadofosveset (MS-325) at 0.03 mmol/kg body weight dose: Phase II and Phase III clinical trials data. Invest Radiol. 2006; 41(11):822–830. [PubMed: 17035873]
247. Farace P, et al. DCE-MRI using small-molecular and albumin-binding contrast agents in experimental carcinomas with different stromal content. Eur J Radiol. 2011; 78(1):52–59. [PubMed: 19443159]
248. Farace P, et al. Cancer-associated stroma affects FDG uptake in experimental carcinomas. Implications for FDG-PET delineation of radiotherapy target. Eur J Nucl Med Mol Imaging. 2009; 36(4):616–623. [PubMed: 19093111]
249. Bhowmick NA, N EG, M HL. Stromal fibroblasts in cancer initiation and progression. Nature. 2004; 432(7015):332–337. [PubMed: 15549095]
250. Loeffler M, et al. Targeting tumor-associated fibroblasts improves cancer chemotherapy by increasing intratumoral drug uptake. J Clin Invest. 2006; 116(7):1955–1962. [PubMed: 16794736]
251. Yu M, Tannock IF. Targeting tumor architecture to favor drug penetration: a new weapon to combat chemoresistance in pancreatic cancer? Cancer Cell. 2012; 21(3):327–329. [PubMed: 22439929]
252. https://medicalxpress.com/news/2013-12-mammography-screening-intervals-affect-breast.html, R.S.o.N. America, Editor.

253. http://www.hitachimed.com/self-learning-activity/docs/PelvisImagingModule/?WT.ac=med_mg_cussite_selflear_pelvim.

254. http://medscape.com/viewarticle/740428_ 2.

255. Lemley KV. An introduction to biomarkers: applications to chronic kidney disease. Pediatr Nephrol. 2007; 22(11):1849–1859. [PubMed: 17394023]

256. Group BDW. Biomarkers and surrogate endpoints: preferred definitions and conceptual framework. Clin Pharmacol Ther. 2001; 69(3):89–95. [PubMed: 11240971]

257. Tesch GH. Review: Serum and urine biomarkers of kidney disease: A pathophysiological perspective. Nephrology (Carlton). 2010; 15(6):609–616. [PubMed: 20883281]

258. Wildgruber M, et al. Assessment of myocardial infarction and postinfarction scar remodeling with an elastin-specific magnetic resonance agent. Circ Cardiovasc Imaging. 2014; 7(2):321–329. [PubMed: 24363356]

259. Sanders HM, et al. Morphology, binding behavior and MR-properties of paramagnetic collagen-binding liposomes. Contrast Media Mol Imaging. 2009; 4(2):81–88. [PubMed: 19191276]

Europe PMC Funders Author Manuscripts

Europe PMC Funders Author Manuscripts

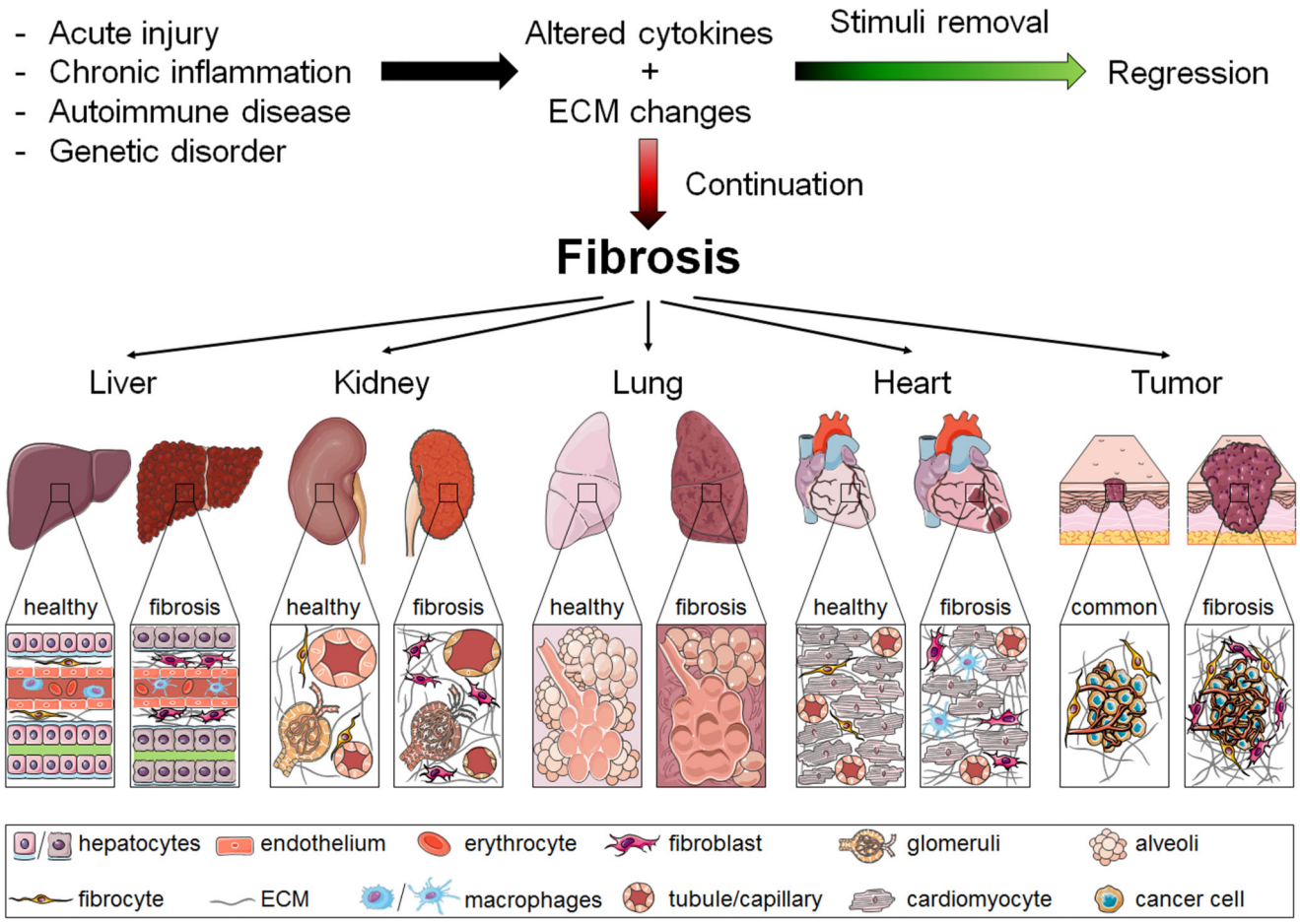

Figure 1.

Pathological characteristics of fibrosis in different tissues. In tissues such as liver, kidney, lung, heart and tumor, common events lead to fibrosis progression (and regression). If the pathological stimulus is persistent and the healing process is dysregulated, the continuous recruitment and activation of inflammatory cells and myofibroblasts can result in fibrosis. Core features of fibrotic processes that are shared by all of these organs include overproduction of cytokines, growth factors, ECM proteins and ultimately the loss of tissue architecture as well as function.

Europe PMC Funders Author Manuscripts

Europe PMC Funders Author Manuscripts

Europe PMC Funders Author Manuscripts

Europe PMC Funders Author Manuscripts

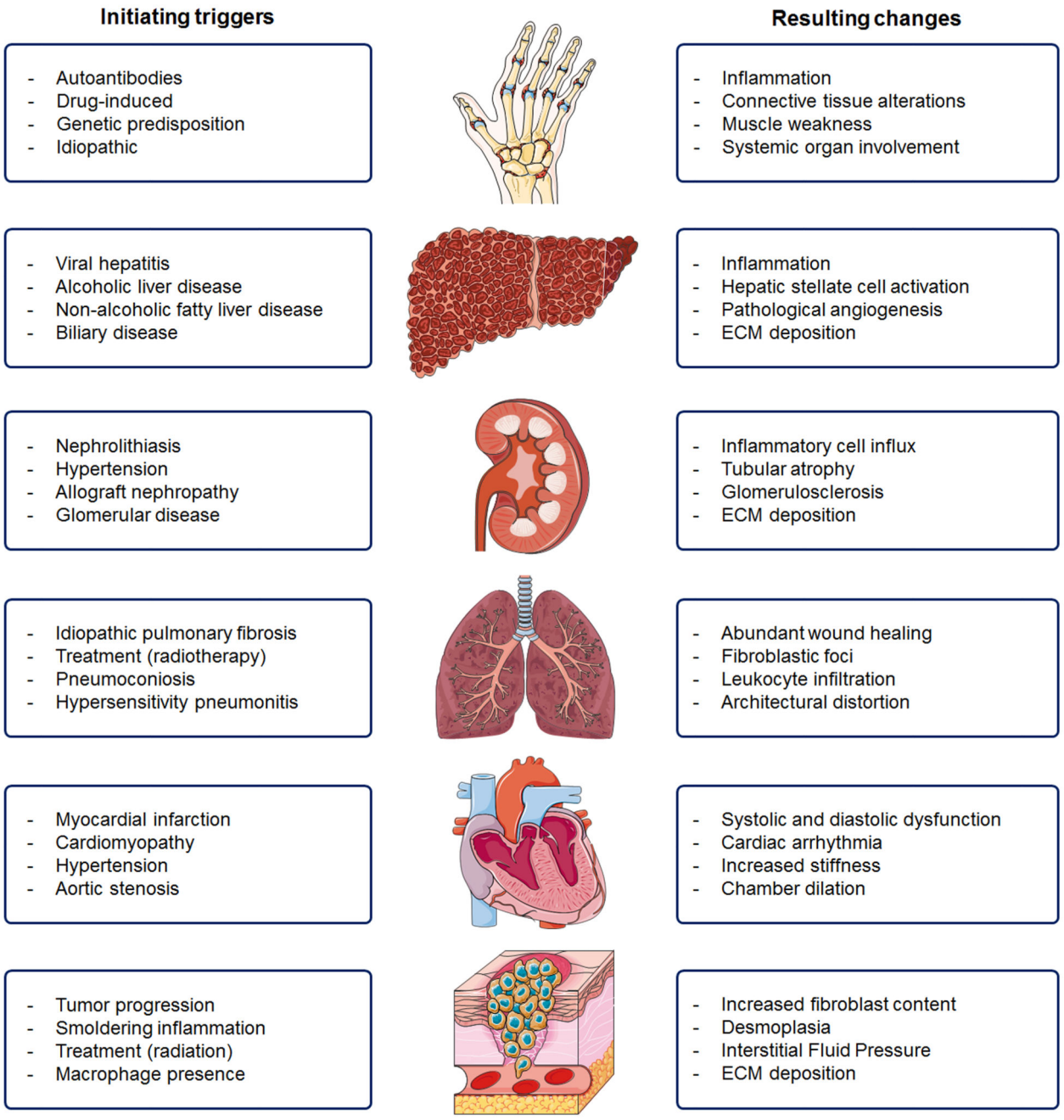

Figure 2.

Causes and consequences of fibrosis in different organs and tissues. A wide range of triggers can induce fibrosis and its progression. These triggers and the resulting changes typically involve (patho-) physiological responses to chronic injury, the induction of innate and/or adaptive immune system, and the recruitment and/or activation of myofibroblasts, which are the primary source of increased deposition of extracellular matrix (ECM) components.

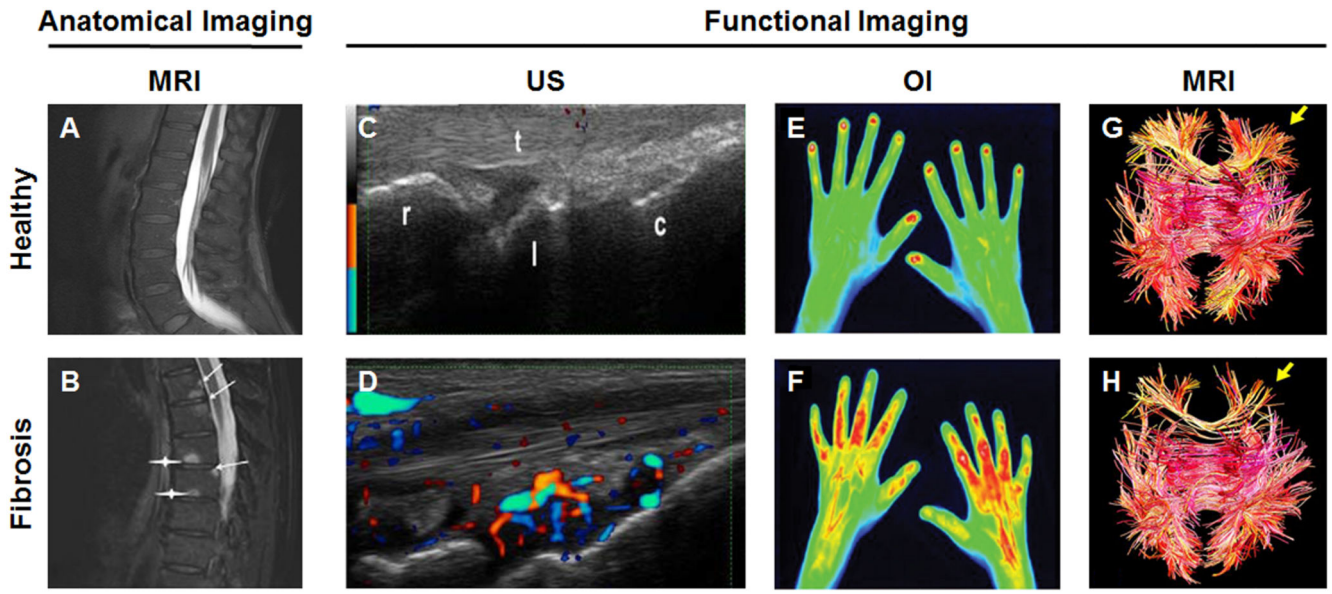

Figure 3.

Imaging of fibrosis-related autoimmune and connective tissue diseases. (A) MRI of a healthy thoracic spine showing no lesions when employing fat suppressed T2-weighted MR sequences. (B) In a patient with ankylosing spondylitis, inflammatory lesions at the center and posterior corners of the vertebral bodies are clearly visible by means of fat suppressed T2-weighted MRI. (C) Semiquantitative color-coded Doppler US images showing a grade 0 healthy wrist with no blood flow. The US image is acquired at the dorsomedial longitudinal axis showing the radius (r), lunate (l), triquetral (t) and capitale (c) bone. (D) Wrist of a patient suffering from grade 3 rheumatoid arthritis, in which color-coded Doppler US shows that more than 50% of the synovial area is filled with blood vessels. (E) Baseline fluorescence levels in healthy control hands after ICG injection acquired with optical imaging. (F) ICG enhancement visualized via optical imaging as an indicator for microvascular damage and endothelial leakiness in the hands of a patient suffering from systemic sclerosis. (G) MRI-DTI-based white matter fiber tractography of a NPSLE patient before treatment. (H) The amount of fibers passing through the frontal brain region is increased after therapy, indicative of a good response (see yellow arrows). Images are adapted, with permission, from [68, 80, 87, 99, 100].

Europe PMC Funders Author Manuscripts
Europe PMC Funders Author Manuscripts

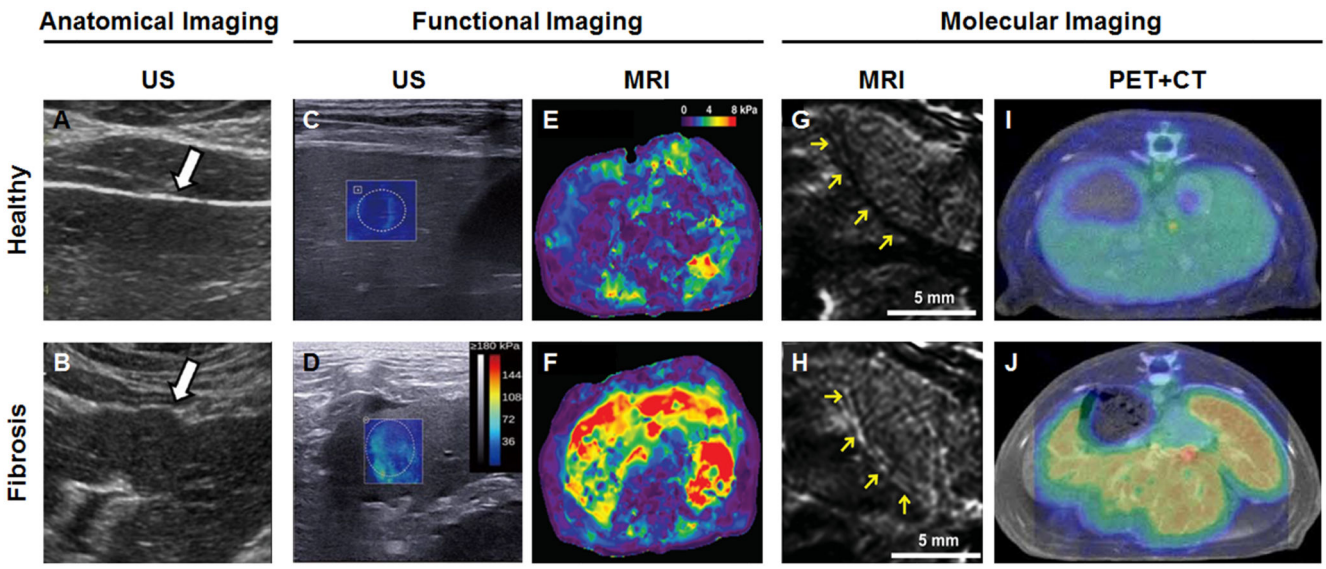

Figure 4.

Imaging of liver fibrosis. (A) Anatomical US imaging depicting the smooth surface of a healthy liver. (B) Anatomical US imaging in case of a fibrotic liver shows an irregularly shaped surface with clearly discernable nodules. (C) Shear wave US elastography of a healthy liver demonstrating low tissue stiffness. (D) High stiffness is detected in a fibrotic liver. (E-F) MRI-based elastrography highlighting the potential of discriminating liver steatosis (E) from a fibrotic liver (F) which typically shows a much higher tissue stiffness. (G-H) T1-weighted MRI upon the intravenous injection of the gadolinium-containing elastin-specific contrast agent ESMA showing no perivascular enhancement in healthy mouse liver (G) and relatively strong perivascular enhancement was observed in the perivascular regions of a fibrotic mouse liver (H). (I-J) The translocator protein-specific radiotracer ^{18}F-FEDAC shows no detectable signal in PET-CT scans in the liver of healthy rats, while significant tracer accumulation is observed in the fibrotic livers of in CCl_4-treated rats (J). Image adapted, with permission, from [103, 112, 116, 126, 132].

Europe PMC Funders Author Manuscripts
Europe PMC Funders Author Manuscripts

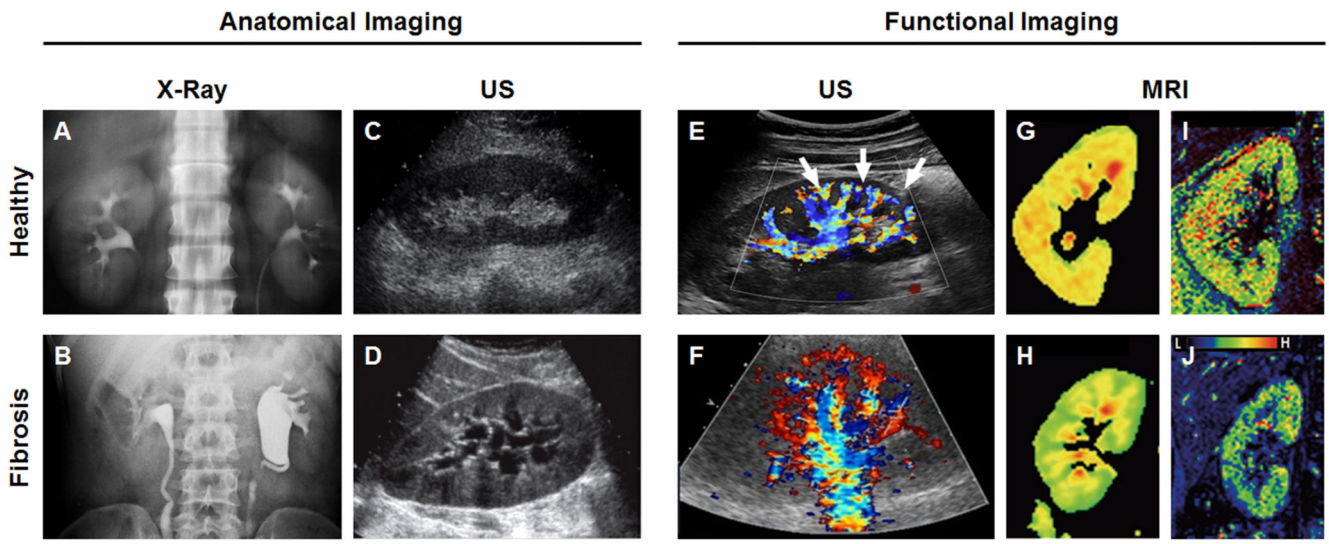

Figure 5.

Imaging of kidney fibrosis. (A) Intravenous x-ray urography depicting filtration of a radiopaque contrast agent through healthy kidneys. (B) X-ray urography showing obstructed contrast agent elimination in case of renal fibrosis. (C) B-mode US imaging highlighting the hypoechoic renal cortex and echogenic fatty tissue associated with renal sinus in a healthy volunteer. (D) In a patient with renal fibrosis, several hypoechoic regions can be observed as a result of inefficient drainage of urine from the kidney to the bladder. (E) Doppler US imaging showing physiologically normal blood flow velocities in a healthy kidney. (F) In renal fibrosis, significant decreases in kidney perfusion can be observed as a result of vessel compression. (G) DWI-MRI demonstrating relatively high diffusivity of water molecules in a healthy kidney. (H) The diffusivity of water molecules as assessed by DWI-MRI is significantly decreased in case of renal fibrosis. (I) BOLD-MRI depicting physiological oxygenation in a healthy kidney. (J) Kidney fibrosis results in a strong decrease in oxygenated blood, which can be visualized and quantified using T2*-based BOLD-MRI. Image adapted, with permission, from [19, 135, 140, 151, 155].

Europe PMC Funders Author Manuscripts
Europe PMC Funders Author Manuscripts

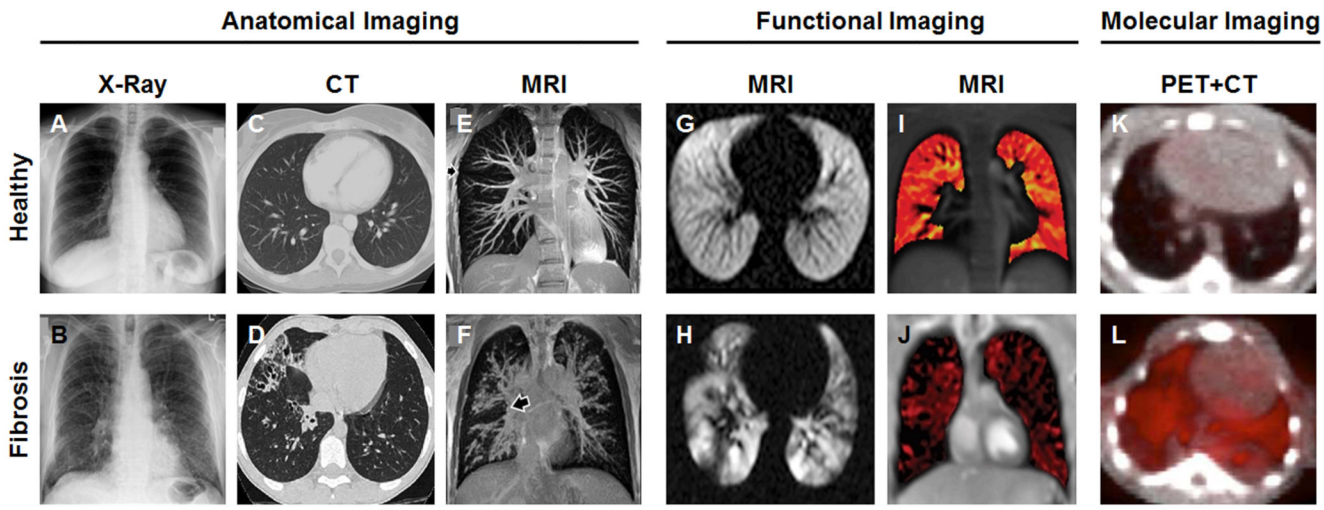

Figure 6.

Imaging of lung fibrosis. (A-B) Anatomical x-ray images depicting dark and non-dense healthy lung tissue (A) and decreased lung volume and reticular opacification in a patient with pulmonary fibrosis (B). (C-D) CT scans showing normal respiratory bronchioles and a lack of air spaces in healthy lungs (C), while in case of fibrosis, dilated and thickened respiratory bronchioles along with large cystic air spaces are observed (D). (E-F) 3D pulmonary MR angiography of a healthy lung depicting well-defined vessels (E), as compared to a fibrotic lung which characterized by inflamed, enlarged and undefined vessels (F). (G-H) The use of hyperpolarized ^{129}Xe as an MRI contrast agent enables visualization of homogeneous ventilation in a healthy volunteer (G), while in a patient suffering from cystic fibrosis, ^{129}Xe-enhanced MRI depicts clear inhomogeneities in the ventilation pattern. (I-J) Self-gated non-contrast enhanced functional lung MRI allows for the assessment of ventilation patterns in healthy individuals (I) and cystic fibrosis patients (J) without the need of administering contrast agents. (K-L) In healthy lungs, no accumulation of the collagen-specific PET probe ^{68}Ga-CBP8 probe is detected, while in mice with bleomycin-induced pulmonary fibrosis, the uptake of ^{68}Ga-CBP8 is clearly visible. Images adapted, with permission, from [157, 162, 167, 172, 179, 180].

Europe PMC Funders Author Manuscripts
Europe PMC Funders Author Manuscripts

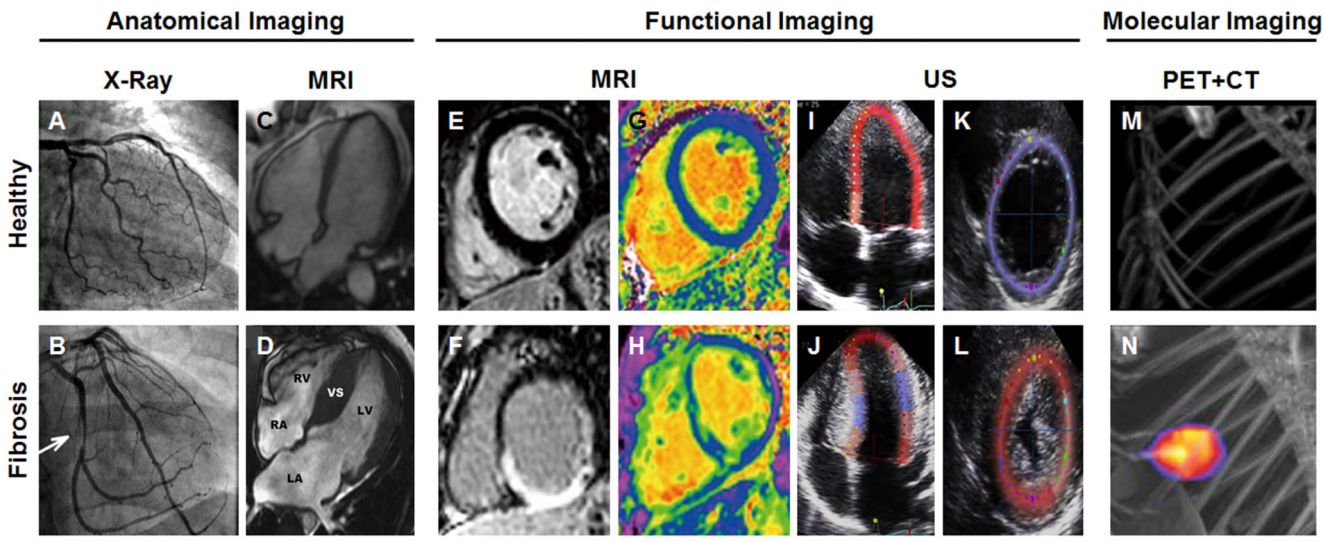

Figure 7.

Imaging of cardiac fibrosis. (A) X-ray coronary angiography of a healthy heart showing no luminal narrowing. (B) In case of cardiac fibrosis, a non-occlusive intraluminal filling in the right coronary artery can be detected by x-ray luminography. (C) Four-chamber end-diastolic CMR image of a healthy heart. (D) Predominant ventricular septal hypertrophy in a patient suffering from hypertrophic cardiomyopathy. The interventricular septum (VS) around the left ventricle (LV) is substantially increased. The other abbreviations indicate left atrium (LA), right atrium (RA) and right ventricle (RV). (E-F) Late gadolinium enhancement (LGE) MRI is frequently employed to assess cardiac scar tissue. Due to differences in washout kinetics, intravenously administered gadolinium-based contrast agents remain shorter in healthy tissue (E) than in areas of replacement fibrosis (F). (G) Normal extracellular volume (ECV) map, which is determined as the ratio of the interstitial volume to the total myocardial volume. (H) In reactive interstitial fibrosis, the ECV map shows heterogeneities across the left ventricular myocardium. The myocardial areas depicted in green represent elevated ECV values. (I-L) Peak systolic strain assessment using speckle tracking echocardiography of the left ventricular global longitudinal strain (I) and of the radial short-axis strain (K) in a control subject. (Four-chamber left ventricular strain assessment in a patient with hypertrophic cardiomyopathy indicating a global strain reduction of 7% (J), which is confirmed in the radial strain view as well as the reduced aortic valve closure (L). (M-N) Maximum-intensity PET-CT images of activated platelet visualized using the integrain-targeted molecular imaging agent $scFv_{anti\text{-}GP2b/3a}$-^{64}CuMeCOSar. No uptake of the radiotracer is detected in sham-operated mice (M), while strong accumulation is observed in ischemic myocardium (N). Images adapted, with permission, from [184, 189, 214, 227–229].

Europe PMC Funders Author Manuscripts
Europe PMC Funders Author Manuscripts

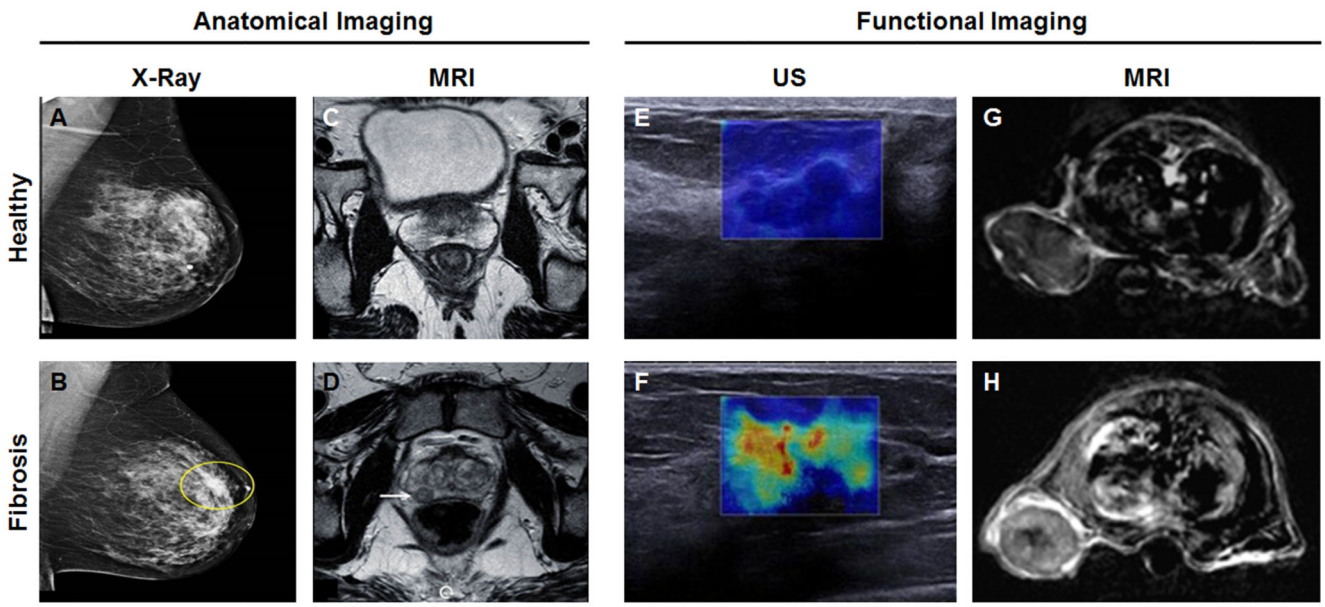

Figure 8.

Imaging fibrosis in tumors. (A) X-ray mammography scans of a healthy breast, depicting fatty tissue as dark areas and denser tissues such as ducts, lobes and glands as bright areas. (B) In case of breast cancer (encircled), thick fibrous connective tissue and calcifications appear as dense bright spots. (C) T2-weighted MRI of a healthy prostate, showing higher intensity signals in the peripheral zones which have a high fluid content. (D) In case of prostate cancer, the same region is characterized by a lower signal intensity signal, indicative of the presence of a fibrotic tumor. (E) SWE US image of a breast showing a homogeneously soft benign lesion. (F) A fibrotic malignant breast lesion is detected using SWE US imaging as a mass with highly heterogeneous stiffness. (G-H) DCE MRI scans after the administration of the albumin-binding contrast agent MS-325 showing relatively low contrast enhancement in non-fibrotic DU-145 tumors (G) and strong contrast enhancement in case of fibrotic BxPC-3 tumors. Image adapted, with permission, from [247, 252–254].

Europe PMC Funders Author Manuscripts
Europe PMC Funders Author Manuscripts

Europe PMC Funders Author Manuscripts

Europe PMC Funders Author Manuscripts

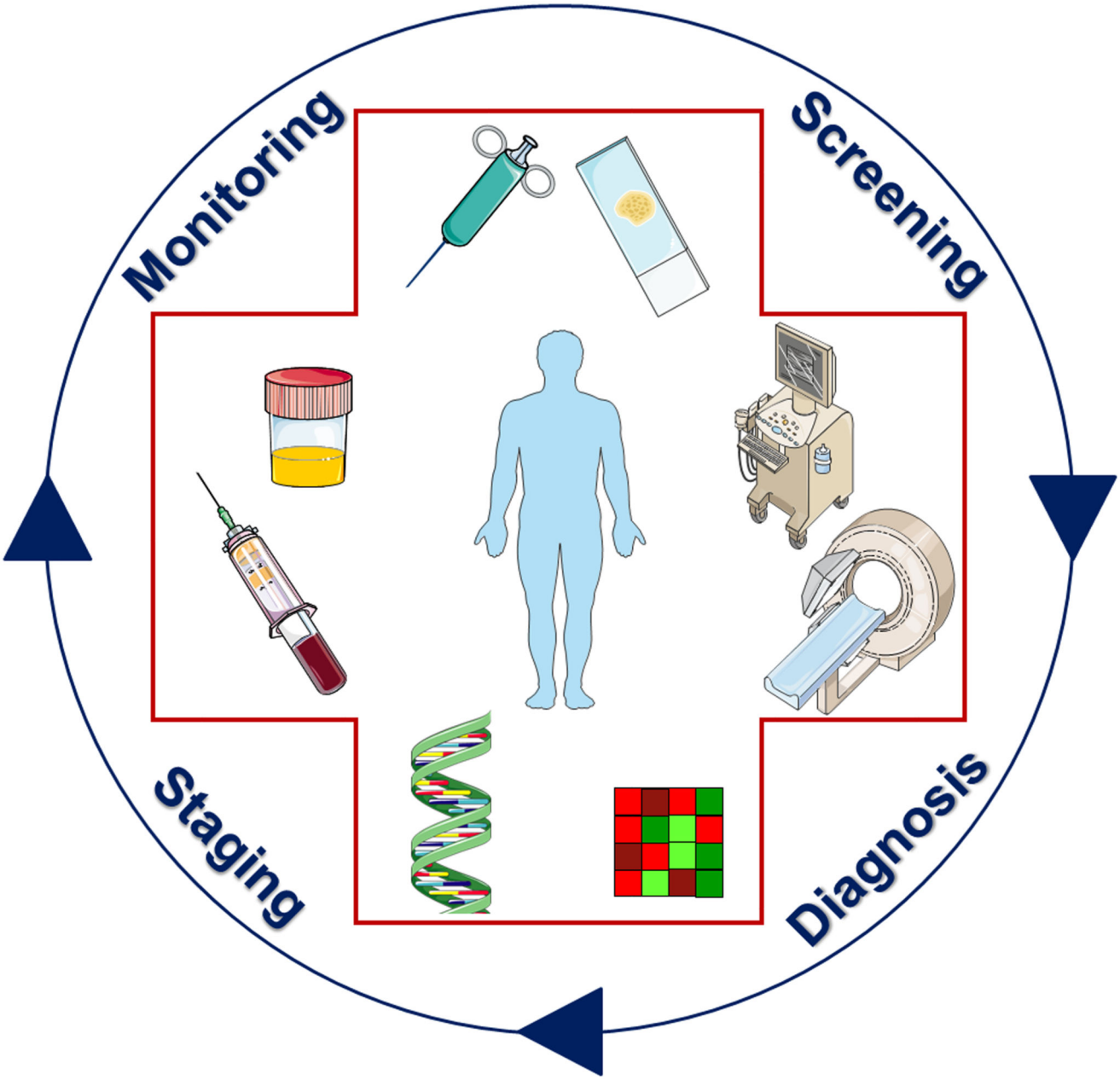

Figure 9.

Schematic setup illustrating how biomarkers can be employed to improve patient management and therapy responses in fibrosis. By combining multiple biomarkers, obtained via tissue- and liquid-based biopsies as well as via imaging, more accurate diagnosis and staging can be performed, and treatments can be individualized and improved.